

SnAKE: Bayesian Optimization with Pathwise Exploration

Jose Pablo Folch¹ Shiqiang Zhang² Robert M Lee³ Behrang Shafei³ David Walz³ Calvin Tsay²
Mark van der Wilk² Ruth Misener²

Abstract

Bayesian Optimization is a very effective tool for optimizing expensive black-box functions. Inspired by applications developing and characterizing reaction chemistry using droplet microfluidic reactors, we consider a novel setting where the expense of evaluating the function can increase significantly when making large input changes between iterations. We further assume we are working asynchronously, meaning we have to decide on new queries before we finish evaluating previous experiments. This paper investigates the problem and introduces ‘Sequential Bayesian Optimization via Adaptive Connecting Samples’ (SnAKE), which provides a solution by considering future queries and preemptively building optimization paths that minimize input costs. We investigate some convergence properties and empirically show that the algorithm is able to achieve regret similar to classical Bayesian Optimization algorithms in both the synchronous and asynchronous settings, while reducing the input costs significantly.

1. Introduction

We introduce a method which seeks to carry out black-box optimization while keeping input variations as small as possible. A black-box function is expensive to evaluate (with respect to time or resources) and we do not have access to gradients. Classically, black-box optimization finds an optimum by sequentially querying the function.

This paper studies a variation of this problem, with two important differences. First, we introduce the idea that large changes in inputs, between iterations, cause the function to become more expensive to evaluate. Second, we do not assume observations are available immediately: a delay between querying the function and getting a result leads to asynchronous decision making.

¹Department of Mathematics, Imperial College London, United Kingdom ²Department of Computing, Imperial College London, United Kingdom ³BASF SE, Ludwigshafen, Germany. Correspondence to: Jose Pablo Folch <jose.folch16@imperial.ac.uk>.

As a motivating example, consider a droplet microfluidic reactor (Teh et al., 2008) (see Figure 1). In such a reactor, we can quickly pump in chemicals, expose them to certain conditions, and collect the results of our experiments as they leave. However, large changes in temperature mean that the reactions are no longer in steady-state and this makes the evaluations unreliable until the system stabilizes. Smaller changes mean that we never leave steady state, or that the system is easier to stabilize. Further, we have to wait for droplets to exit the reactor before obtaining observations.

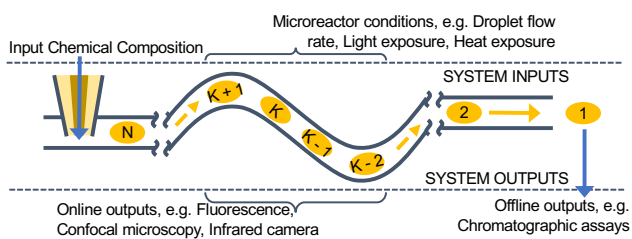


Figure 1. Motivating example. Droplets flow into the micro-reactor where we control conditions such as temperature and flow rate. The cost to change function inputs arises from how adjacent droplets are coupled, e.g. rapidly changing the temperature after droplet K means waiting for system equilibration before taking new measurements. Asynchronicity arises from choosing drops 2, 3, ..., N before getting the results of droplet 1.

Classical Bayesian Optimization (BO) (Jones et al., 1998; Shahriari et al., 2016) provides effective solutions to black-box optimization. However, by nature BO follows a ‘greedy’ approach, in that BO chooses the next query based only on the current state of the surrogate model. This leads to a lot of input space ‘jumps’, as BO reduces uncertainty in unexplored areas and then jumps back to promising areas with no regard for the distance between consecutive query points in the input space. This means that BO will incur very high *input costs*, \mathcal{C} .

However, having zero changes in input space is obviously not a good solution. After all we want to explore the search space to find the optimum point. We seek an algorithm that preserves the essence of Bayesian Optimization. Consider a scenario where we can see into the future, so that we know beforehand which points classical BO would query. In this case, we could simply order the queries to attain the

smallest input cost. In other words, a good solution would require looking into the future, creating an ordering, and then simply following the *path* defined by the ordering.

As we do not have access to the relevant information from the future, perhaps we can find an *approximate* idea of how the future looks. Using this information, we begin evaluating the objective function in an ordered manner. Once we start obtaining new information, we could update our beliefs and update our optimization path.

This paper proposes *Sequential Bayesian Optimization via Adaptive (K)Connecting Samples* (SnAKe). Just as the snake grows by carefully eating items in the classic arcade game, a SnAKe optimization path grows from carefully adding queries to the evaluation path.

2. Related Work

‘Process-constrained Batch Bayesian Optimization’ (Vellanki et al., 2017), is the closest analog to our setting of BO with input costs. Vellanki et al. (2017) navigate the physical limitations in changing the input space (cost metric \mathcal{C}) by *fixing* the complicated inputs for every batch. Rather than fixing the difficult-to-change inputs, we *penalize* large input variations in line with the costs (time and resources) of changing conditions. SnAKe decides when to make expensive input changes. Waldron et al. (2019) compare the use of transient variable ramps (small input changes in a manually pre-determined manner) against a full steady-state design of experiments approach for learning parameters of chemical kinetic models. They show that the transient approaches give less precise estimates but much faster. SnAKe combines the best of both worlds, automatically designing experiments while keeping input changes small.

Asynchronous Bayesian Optimization (Kandasamy et al., 2018; Alvi et al., 2019) addresses the problem of choosing queries while waiting for delayed observations. To the best of our knowledge, there has never been a consideration of the input costs incurred when selecting the queries. The idea of anticipating the course of the optimization is known as *look ahead* Bayesian Optimization (Lam et al., 2016; González et al., 2016b). By considering possible future queries, we can make our current choice less myopic. Usually one only looks ahead for a few iterations, due to the computational complexity of looking too far ahead into the future (Yue & Kontar, 2020).

3. Methods

3.1. Problem Set-up

We consider maximizing a black-box function, f :

$$x^* = \arg \max_{x \in \mathcal{X}} f(x) \quad (1)$$

where \mathcal{X} is a compact subset of \mathbb{R}^d . We assume f is continuously differentiable, and that this function is expensive to evaluate. We seek the optimum point while keeping the number of evaluations small.

We evaluate the function sequentially, over a discrete number of samples, $t = 1, \dots, T$. For every query, x_t , we obtain a noisy observation, y_t , of our target objective:

$$y_t = f(x_t) + \eta_t \quad (2)$$

where $\eta_t \sim \mathcal{N}(0, s^2)$ is Gaussian noise. We assume there is delay, t_{delay} , between choosing a query and getting an observation. So our data-set at time t is given by $D_t = \{(x_i, y_i) : i = 1, \dots, t - t_{delay} - 1\}$. If we set $t_{delay} = 0$, we revert to classical sequential Bayesian Optimization, otherwise we are in an *asynchronous* setting.

Finally, we assume there is a *known* inherent cost to changing the inputs to our evaluation, $\mathcal{C}(x_t, x_{t+1})$. We want to minimize regret while keeping $\sum_{t=1}^{T-1} \mathcal{C}(x_t, x_{t+1})$ small.

3.2. General Approach

For our general approach, we will seek to create a *batch* of queries that *approximates* the whole optimization procedure. This is useful for two reasons: first, it allows us to order the queries in a way that reduces input cost. Second, it allows us to deal with any delay in getting observations, because we can pre-select future queries.

Once the batch is defined, we will order it such that the input cost is minimized. We will then follow this ordering or path until new information is available, after which we will update our path.

Algorithm 1 General Ordering-Based Optimization

input Optimization budget of T samples. Method for creating batch of queries. Method for creating an ordering from a batch of queries. Method for updating paths.
Begin algorithm:
 Create initial batch of size T and ordering, S
for $t = 1, 2, 3, \dots, T$ **do**
 if there is new information **then**
 Update surrogate model
 Choose a batch of new points to query
 Create a new path, \tilde{S}
 $S \leftarrow \tilde{S}$
 end if
 Choose next query point from ordering: $x_t \leftarrow S_t$
 Evaluate $f(x_t)$
end for

3.3. Modeling the function

To model the black-box function, we put a Gaussian Process (GP) prior on $f \sim \mathcal{GP}(\mu_0, \sigma_0^2)$. Since we have Gaussian noise, the posterior, $f|D_t$ is also a GP, whose mean function, $\mu_t(\cdot)$, and variance, $\sigma_t^2(\cdot)$ can be calculated analytically (Rasmussen & Williams, 2005).

3.4. Creating a Batch Through Thompson Sampling

There are many proposed methods for Batch Bayesian Optimization (BBO) (González et al., 2016a; Azimi et al., 2010). However, other BBO approaches query all the proposed points. Unless t_{delay} is longer than T , the total number of samples, we are not interested in querying all the points in the batch. Instead, once the surrogate model is updated, Algorithm 1 creates a new batch. Each batch simply works as a guide for what the future might look like.

González et al. (2016b) and Jiang et al. (2020) link BBO with predictions of the future, using a Local Penalization method (González et al., 2016a) and Expected Improvement (q-EI) (Ginsbourger et al., 2010) respectively. Unfortunately, they restrict themselves to smaller batch sizes ($q \leq 15$) due to computational expense.

We require a method capable of producing batches that are representative of the current state of the surrogate model. Not only this, but the method should allow for big batch sizes, since we want to produce batches as big as our budget (which is usually much larger than the batch size most methods consider). For example, in a micro-reactor, we might be interested in batches that contain hundreds of points (Teh et al., 2008).

Kandasamy et al. (2018) offers a promising solution where every point in the batch is independent. The method is based on Thompson Sampling, which uses the GP’s own randomness to create a batch. A single batch point is chosen by drawing a realization of the GP, and optimizing it.

The queries will fill out the space, and they are more likely to be on promising, and unexplored areas. It should work very well in our context given we expect our initial batch sizes to be very large, so the sample should be representative of the current state of our surrogate model.

3.5. Creating a Path via the Travelling Salesman Problem

After selecting a batch of queries, $\mathcal{P}_t = \{x_t^{(i)}\}_{i=1}^{\tilde{T}}$, we order them. We do this by embedding a graph into the batch, where the edge weights are the cost for changing one input to another. We then find the shortest path that visits every point, i.e., solve the Travelling Salesman Problem (TSP) (Bellman, 1962; Dorigo & Gambardella, 1997). We discuss the problem of computational cost, and practical approaches

later.

To be more precise, we define the graph $G = (V, E, W)$, with $V = \{i \in 1, \dots, \tilde{T} : x_t^{(i)} \in \mathcal{P}_t\}$, $E = \{(i, j) : i, j \in 1, \dots, \tilde{T}\}$, and $W = \{w_{ij} = \mathcal{C}(x_t^{(i)}, x_t^{(j)}) : (i, j) \in E\}$, where \tilde{T} is the number of batch samples. We solve the TSP in G to obtain our latest optimization path. A simple example would be to try to minimize the total distance travelled in input space, by selecting the Euclidean norm as cost $\mathcal{C}(x_t, x_{t+1}) = \|x_t - x_{t+1}\|$.

3.6. Naively Updating the Optimization Path

After updating the GP with new observations, we want to use this information to update our path. We propose updating our strategy by creating a new batch of points.

At iteration t , we have a remaining budget of size $T - t$. We first propose sampling $T - t$ queries through Thompson Sampling, and then solving the Travelling Salesman Problem. However, we will see this leads to the algorithm getting ‘stuck’ in local optima. This is because every time we re-sample, we naturally include *some exploitation* in the batch, and this exploitation will always be the next point chosen by the TSP - we will never reach the *exploration* steps of the algorithm. See Figure 2a for an example.

3.7. Escape Analysis

To try and solve the convergence problem introduced by naively resampling, we will briefly analyze it theoretically. For this analysis, assume that we receive noise-less observations. However, all the sampling can be done in the presence of noise by calculating the corresponding posterior. We focus on the Thompson Sampling distribution.

Definition 3.1. (Thompson Sample) We say $x_t^{(i)}$ is Thompson Sampled, and we write $x_t^{(i)} \sim \tau_t$, if:

$$f_t^{(i)}(\cdot) \sim \mathcal{GP}(\mu_t, \sigma_t | D_t)$$

$$x_t^{(i)} = \arg \max_{x \in \mathcal{X}} f_t^{(i)}(x)$$

Note that the sampling distribution changes at each iteration.

One particular concern, diagrammed in Figure 2a, is the possibility of the method being stuck in a certain area. Let $A = B_\delta(a)$ be a Euclidean δ -ball centered at a . Assume further that $x_{t-1} \in A$.

Definition 3.2. (Non-escape Probability) We define the non-escape probability, p_t , at time t , as the probability of a Thompson Sample falling into A . That is, for $x_t^{(i)} \sim \tau_t$:

$$p_t = \mathbb{P}(x_t^{(i)} \in A) = \mathbb{P}(\|x_t^{(i)} - a\| \leq \delta) \quad (3)$$

Let $\mathcal{P}_t = (x_t^{(1)}, \dots, x_t^{(T-t)}) \sim \tau_t$ *i.i.d.*. Of particular interest to us, is the number of ‘non-escapes’ in the sample,

$N_t = |\mathcal{P}_t \cap A|$. We are guaranteed to escape if no sample falls in A , so we say we have *fully escaped* if $x_t^{(i)} \notin A \forall i$.

Lemma 3.3. *The probability of fully escaping is $(1 - p_t)^{T-t}$.*

Proof. The probability of fully escaping is:

$$\mathbb{P}(x_t^{(i)} \notin A \forall i) = \mathbb{P}(N_t = 0) = (1 - p_t)^{T-t}$$

This follows from the fact that $N_t \sim \text{Binomial}(T - t, p_t)$ as all the samples are mutually independent. \square

From the Lemma, we learn that we can only expect to fully escape if p_t is very small. Therefore we are interested in the behavior of p_t as we gain more and more information about f in A .

For the next part of the analysis, we consider the circumstances under which p_t becomes very small.

3.7.1. AREAS WITHOUT STATIONARY POINTS

Consider a δ -ball $A = B_\delta(a)$ around a , such that the ball does not contain any stationary points. Then the maximum of f on the closure of the ball, \bar{A} , must lie on the boundary of the ball. In particular, if we assume that our Gaussian Process model has no error in A , and assuming continuity of sample paths, then it must be that $p_t = 0$.

Intuitively, the area itself contains enough information to ensure, with complete certainty, that the global optimum does not lie in the area. We hope that, as we collect information inside areas without stationary points, $p_t \rightarrow 0$, and we will eventually leave them with small probability of returning. Appendix A.2 shows an example of this happening very fast.

3.7.2. AREAS WITH STATIONARY POINTS

Areas with stationary points pose a much bigger problem. We will restrict our arguments to local maximums since this is where we have observed the problem. Assume that A is an area which contains a local optimum higher than any other we have observed before. In this case, any sample taken from a Gaussian Process with no error in A will have a local maximum inside A , and therefore it is possible that this local maximum is the global solution.

As we increase the information inside the area, p_t is not guaranteed go down to zero. This makes intuitive sense; the only way of knowing if a local optimum is not a global optimum is by sampling away from it - therefore with limited information we will allocate a certain probability to the global optimum being inside A . We include a clear example where $p_t \rightarrow p > 0$ in Appendix A.1.

Sampling consistently in a promising area is not necessarily a bad thing, indeed we want to exploit near possible global optimums. However, the question then becomes, how long will it take us to leave? Recall the probability of fully escaping is $(1 - p_t)^{T-t}$, and therefore it will be increasing as t increases, even if p_t is (almost) constant.

Remark 3.4. Assume we have a high escape probability after t_e iterations, i.e. $(1 - p_{t_e})^{T-t_e}$ is large, leaving us $T - t_e$ iterations to explore the rest of the space. If we increase our budget from T to T' , we will not have a high probability of escape until $(1 - p_t)^{T'-t} = (1 - p_t)^{T-t_e}$, i.e. $t = T' - T + t_e$. This leaves us with $T' - T' + T - t_e = T - t_e$ iterations to explore the rest of the space. Increasing our budget *does not* increase our budget after leaving A ! It only means we will be stuck in A for a longer time. This is very concerning as the method will be very myopic; if it finds a local optimum, it is likely that it will spend a very large amount of the budget exploiting it.

3.8. Escaping with ϵ -Point Deletion

The convergence problem stems from the fact that we require $N_t = 0$ to be able to fully escape. As a solution, we propose sampling more points than we need, and then deleting batch points that are similar to previously explored points. Algorithm 2, which we dub ϵ -Point Deletion, still allows us to exploit local optima if we sample many points near them, however, it should eventually move on.

Note that Point Deletion uses the Euclidean norm, and it is independent of the cost function. This is because we are trying to escape local minima of simple regret.

Algorithm 2 ϵ -Point Deletion

```

input New proposed batch  $\mathcal{P}_t$  (size  $T$ ), set of already
queried points  $Q_t$  (size  $t$ ), and deletion distance  $\epsilon$ 
for  $x \in Q_t$  do
   $\tilde{d} \leftarrow \min_{x' \in \mathcal{P}_t} \|x - x'\|$ 
  if  $\tilde{d} < \epsilon$  then
    # find the closest point to the
    query  $x$  in the new batch
     $\tilde{x} \leftarrow \arg \min_{x' \in \mathcal{P}_t} \|x - x'\|$ 
  else
    # else pick a random sample
     $\tilde{x} \leftarrow \text{Random}(\mathcal{P}_t)$ 
  end if
  # remove said point from the batch
   $\mathcal{P}_t \leftarrow \mathcal{P}_t \setminus \{\tilde{x}\}$ 
end for
output A batch  $\mathcal{P}_t$  (size  $T - t$ )

```

ϵ -Point Deletion allows us to escape local optima by directly increasing the probability of fully escaping without changing p_t . To see this, consider the case where there

are q_t previously queried points inside the ball, A , and set $\epsilon \geq 2\delta$. Then it follows that we will escape if we have less than q_t Thompson Samples inside A . Notice that $N_t \sim \text{Binomial}(T, p_t)$, since we are oversampling. Therefore the probability of fully escaping has the lower bound:

$$\mathbb{P}(x_t^{(i)} \notin A \ \forall i) \geq \mathbb{P}(N_t \leq q_t) = \sum_{i=0}^{q_t} \binom{T}{n} p_t^i (1-p_t)^{T-i}$$

In particular, consider the expected number of ‘non-escapes’, $\mathbb{E}[N_t] = p_t T$. Around a local maximum, this quantity may be approximately constant with time, $p_t T \approx pT$, so we can reasonably expect an escape when $q_t = pT$. This is a desirable property because we still want to allow exploitation of promising areas. However, this time we leave $T - q_t = T(1 - p)$ extra iterations to explore the remaining space! Increasing the budget will benefit *both* the exploitation and the exploration instead of only the former (in contrast with remark 3.4).

Figure 2 gives an empirical example where we use Point Deletion, with $\epsilon = 0.1$, to escape a local optimum. We observe the expected behavior from our brief analysis. For Point Deletion, we calculate the escape prediction as $pT \approx 74$, using $\hat{p} \approx 0.74$, which we estimated in Appendix A.1. We can see that without Point Deletion, we remain stuck in the first local optimum.

3.9. SnAKE

Algorithm 3 which we dub ‘Sequential Bayesian Optimization via Adaptive Connecting Samples’ (SnAKE), combines the ideas of previous sections. Figure 3 diagrams the most important steps of SnAKE. Section 4 develops an effective, non-parametric alternative to the choice of ϵ .

Note there is no requirement for data to be available immediately following querying. If $t_{delay} > 0$, we can simply stick to the latest path. It works without modification on the asynchronous setting. This is a vital point since we were inspired by chemical experiment design which can exhibit asynchronous behavior.

3.10. Computational Considerations

Unfortunately, Algorithm 3 is computationally expensive in two main aspects. First, for large budgets, we might struggle to train and sample the GPs. For our experiments training was not an issue and we were able to use full model GPs. However, we could use Sparse GPs (Snelson & Ghahramani, 2005) if needed.

The Wilson et al. (2020) approach allows us to create GP samples efficiently, and possibly optimize them using gradient methods. The sampling can be done in linear time (after the GP has been trained). We use the Wilson et al. (2020) method to create our samples, and then optimize the

Algorithm 3 SnAKE

input Optimization Budget, T . Deletion constant, ϵ .

Create initial batch, \mathcal{P}_0 , uniformly. Choose starting point x_0 . $Q_0 \leftarrow \{x_0\}$. Create initial path, S_0 , by solving TSP on \mathcal{P}_0 .

for $t = 1, 2, 3, \dots, T$ **do**

 Check if any running evaluations are finished

if there are new observations **then**

 Update surrogate model

 Create batch of size T using Thompson Sampling,

\mathcal{P}_{t-1}

$\mathcal{P}_{t-1} \leftarrow \epsilon\text{-Point Deletion}(\mathcal{P}_{t-1}, Q_{t-1})$

$\tilde{S} \leftarrow \text{TSP}(\mathcal{P}_t, \text{source} = x_{t-1}) \setminus \{x_{t-1}\}$

$S \leftarrow Q_{t-1} \cup \tilde{S}$

end if

 Choose next query point from schedule: $x_t \leftarrow S_t$

$Q_t \leftarrow Q_{t-1} \cup \{x_t\}$

 Evaluate $f(x_t)$

end for

samples using Adam (Kingma & Ba, 2014).

The second bottleneck is solving the TSP, which is NP-hard, and we may need to solve it almost at every iteration (for small values of t_{delay}). There are heuristic solutions that give approximate solutions quickly. We use Simulated Annealing (Kirkpatrick et al., 1983) which grows linearly with the budget size, T . For small budgets, simulated annealing should find good solutions, but it could struggle as the budget size increases. To solve this, we note that we do not actually require a super-specific solution to the problem: we are only expecting to query the first few points on a path before replacing it by an entirely new path.

We build an adaptive grid (at each iteration) consisting of two separate parts. A very coarse grid, ξ_{global} , covers most of the search space, and a very fine grid, $\xi_{local,t}$, consisting of the N_l samples closest to x_t . This allows us to define the grid $\xi_t = \xi_{global} \cup \xi_{local,t}$. The remaining $T - N_l$ samples will be assigned to the closest point in ξ_t (using the Euclidean distance).

The adaptive grid means we expect to have multiple samples assigned to the same point, specifically in the coarse areas of our grid. But this is not important, because we expect our immediate attention will be in the area around our current input where there should be little to no repetition. This will allow the algorithm to focus on testing solutions which are relevant to our problem.

The adaptive grid introduces two hyper-parameters: the size of the global and local grids, respectively N_g and N_l . Using this method, we run the TSP heuristics on a graph with at most $\min(N_g + N_l, T)$ nodes. For the experiments, we

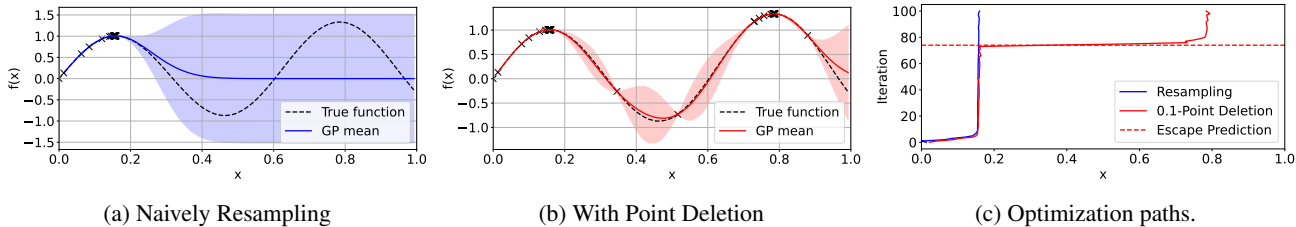


Figure 2. Effect of Point Deletion for ordering-based BO. (a) and (b) show the maximization objective and the underlying surrogate model, with black crosses representing queries and observations. (c) shows the optimization paths. Naive resampling gets stuck in the local optimum ($x = 0.16$) whereas Point Deletion escapes the local solution. We also show the predicted escape time, T_p (after estimating $p \approx 0.74$ in Appendix A.1), which accurately predicts the behavior of the algorithm in this simple example.

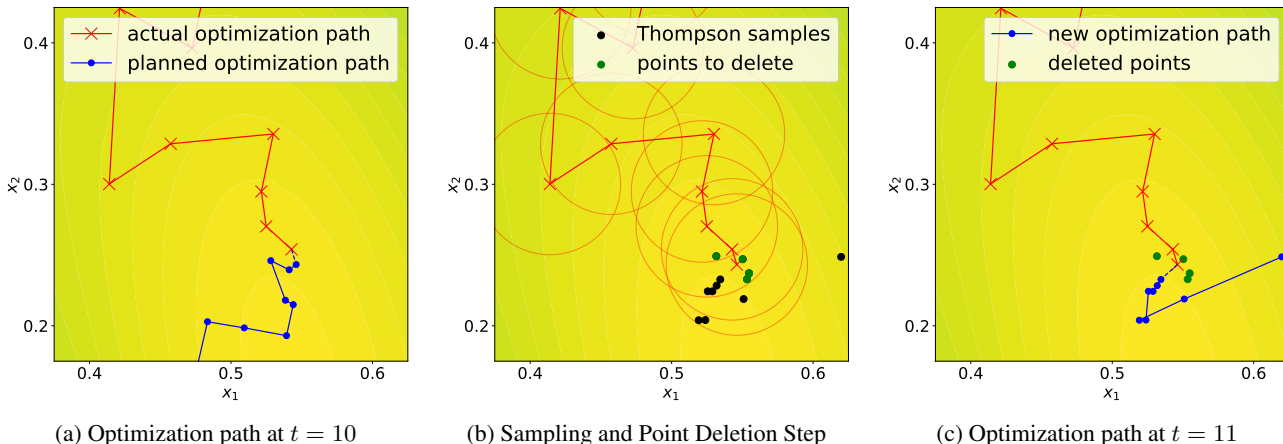


Figure 3. Graphical example of SnAKE behavior in a full iteration if new information is available. The underlying function is Branin 2D. The feasible set is $[0, 1]^2$, so we do not see all the samples or the complete path with this zoomed-in view. (a) The red line shows the path we have already queried. The blue path shows our future plans. (b) For each query, we can see the ϵ -ball under which the deletion step is deterministic. We plot the Thompson Samples as dots, the accepted ones in black and the deleted ones in green. (c) The new path is in blue and the points that were ignored (due to Point Deletion) are in green. Notice how there is a higher concentration of samples in what the model considers a promising area.

create the global grid using a simple Sobol grid (Sobol’, 1967).

4. Experimental Results

For all experimental results we report the mean and the standard deviation over 10 experimental runs. We give the full implementation details and results in Appendix B and C respectively. All classical BO methods are implemented using BoTorch (Balandat et al., 2020) and GPyTorch (Gardner et al., 2018). We will be using simple regret, $SR_t = f(x^*) - \max_{i=1, \dots, t} f(x_i)$ as the performance metric.

In all experiments, we examine SnAKE for $\epsilon = 0, 0.1$, and 1. We further introduce a non-parametric alternative by adaptively selecting ϵ to be the smallest length scale from the GP’s kernel, and denote it ℓ -SnAKE. SnAKE proves to be robust to non-zero choices of ϵ . For $\epsilon = 0$ we observe very low cost, at the expense of some regret.

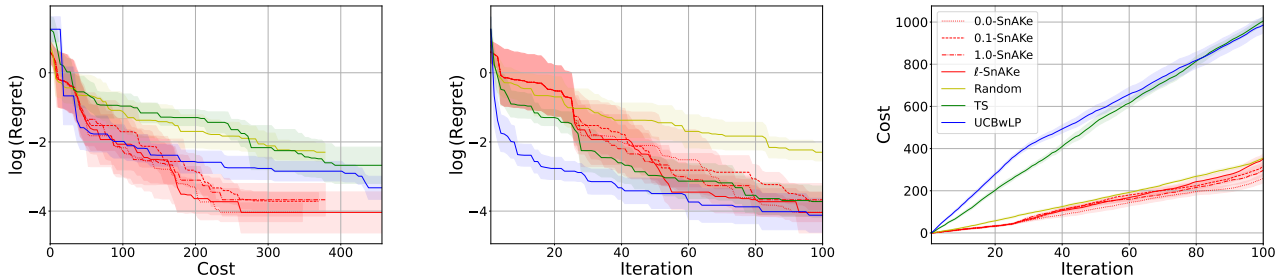
4.1. Synthetic Functions

4.1.1. SEQUENTIAL BO

This section examines the performance of SnAKE against Classical Bayesian Optimization algorithms. We compare Expected Improvement (EI) (Mockus et al., 2014), Upper Confidence Bound (UCB) (Srinivas et al., 2010), and Probability of Improvement (PI) (Kushner, 1964). We also introduce a simple baseline, where we create a random Sobol sample, and then arrange an ordering by solving the TSP, and never update the path again. We do this in six classical benchmark functions. We set the cost function to be the 2-norm distance between the inputs. The results are shown in Figure 5.

4.1.2. ASYNCHRONOUS BO

We explore the asynchronous setting, comparing Local Penalisation with UCB (LPwUCB) (González et al., 2016a; Alvi et al., 2019), Thompson Sampling (TS) (Kandasamy



(a) Evolution of regret against input cost. We can see that SnAKE is able to achieve the best regret for low cost.

(b) Evolution of regret with iteration number. The final regret achieved by SnAKE is comparable with Bayesian Optimization methods.

(c) Evolution of input cost with iteration number. The lowest cost is achieved by SnAKE and the TSP-ordered Random optimization.

Figure 4. Results of experiments on the SnAr chemistry Benchmark. SnAKE is the only method achieving both low regret and low cost. The bounds are created from \pm half the standard deviation of all runs. The best performer, ℓ -SnAKE, is non-parametric.

et al., 2018), and the same Random baseline from the sequential setting. The results are shown in Figure 6.

4.2. Reaction Control on SnAr Benchmark

We test our method on a real-world, SnAr chemistry benchmark (Hone et al., 2017). We control three variables; equivalents of pyrrolidine, concentration of 2,4 dinitrofluorobenzene at reactor inlet, and reactor temperature. We assume changing temperature and concentration incur an input cost, owing to the response time required for the reactor to reach a new steady state. We assume the reactor as a first-order dynamic system, where the response to changes in input is given by:

$$(x_s)_i = (x_t)_i + (1 - e^{-s/\alpha_i})(\Delta x_t)_i \quad (4)$$

Where s denotes the time after experiment x_t is finished, $(x_t)_i$ denotes the i th variable of the t th experiment, $(\Delta x_t)_i = (x_{t+1})_i - (x_t)_i$, and α_i is the system time constant. We assume the system reaches steady state once $|(x_s)_i - (x_{t+1})_i| \leq \beta_i$. For input changes smaller than β_i , we assume a linear cost, defined by a parameter γ_i . Combining the response time from (4) with this linear cost gives an input cost function, $C_i(x_t, x_{t+1})$ of:

$$\gamma_i \min\{\beta_i, |\Delta^{(i)} x_t|\} + \max\left\{0, \alpha_i \log\left(\frac{|\Delta^{(i)} x_t|}{\beta_i}\right)\right\} \quad (5)$$

Finally, we assume that we can change variables simultaneously, so the total input cost is simply the longest response time within a given set of input changes. That is:

$$C(x_t, x_{t+1}) = \max_{i \in I_c} C_i(x_t, x_{t+1}) \quad (6)$$

Where I_c is the index set of the control variables. We implement the simulation using the Summit package (Felton et al., 2021). We control temperature between 40 and 120 degrees, and concentration from 0.1 to 0.5 moles per liter. We set the

cost parameters for temperature $\alpha_{temp} = 5, \beta_{temp} = 1, \gamma_{temp} = 1$, and the cost parameters for concentration $\alpha_{conc} = 2, \beta_{conc} = 0.01, \gamma_{conc} = 1$.

Finally, we assume a measurement delay of $t_{delay} = 25$, and we optimize for $T = 100$ iterations. The results of the experiment can be seen in Figure 4.

5. Conclusion and Discussion

This paper introduces and proposes a solution to the problem of optimizing black-box functions under costs to changes in inputs. We have empirically shown that the regret achieved by our method is comparable to those of classical Bayesian Optimization methods and we succeed at achieving considerably lower input costs.

This setting, with input costs penalizing experimental changes, makes a major step towards automating new reaction chemistry discovery, e.g. in line with the vision of Lazzari et al. (2020). We substantially decrease experimental cost with respect to classical black-box optimization, e.g. as used by Fath et al. (2021) and McMullen & Jensen (2011). In the real-life SnAR benchmark, SnAKE spends 30-40% of the cost while making similarly strong predictions to classical BO. The synthetic benchmarks offer similar advantages.

Beyond the importance to applications, the path-based solution to SnAKE offers an interesting hybrid between black-box and gradient-based optimization approaches. As in black-box optimization, the function is expensive to query and we do not have enough budget to approximate a gradient using finite difference schemes. Although we are missing these gradients, the path-based nature of our approach required us to explicitly treat the possibility of getting trapped in local solutions (a common challenge in gradient-based optimization). We can view path-based BO as therefore adopting features of gradient-based methods.

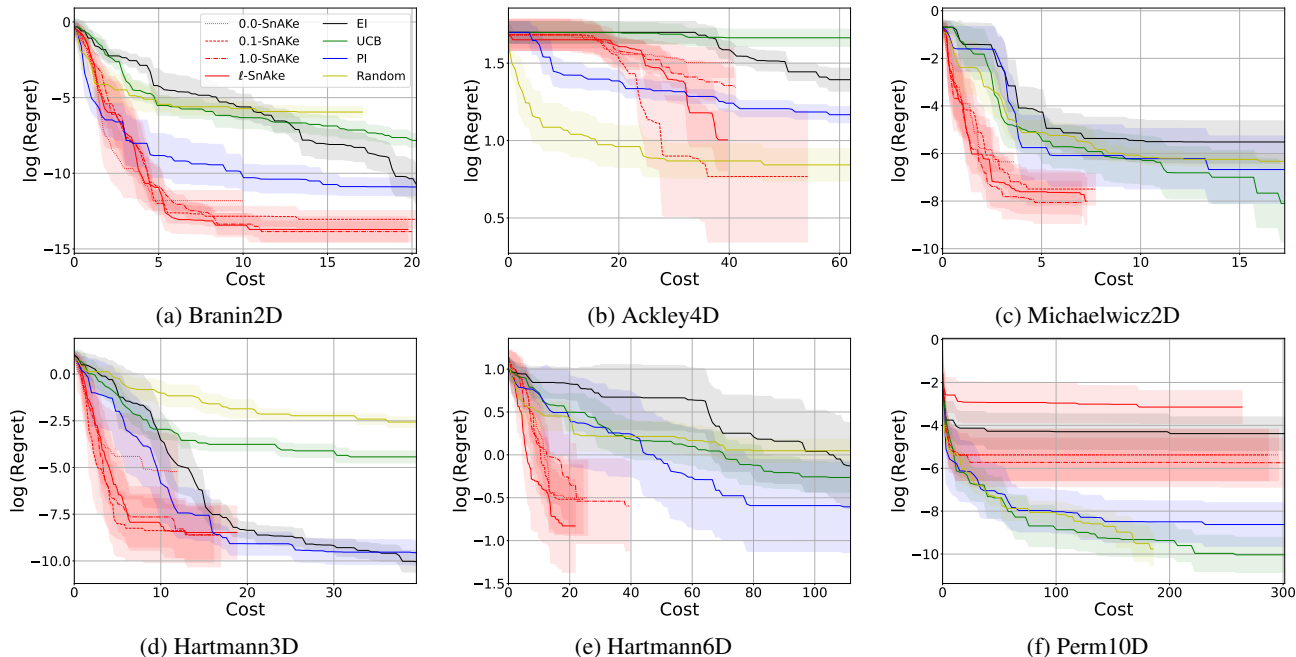


Figure 5. Results of synthetic experiments. We plot the average $\log(\text{regret})$ achieved against the cost spent. For every experiment we set $T = 250$, and limit the x -axis to the maximum cost achieved by SnAKE or Random. l -SnAKE is the non-parametric version of the algorithm. SnAKE only struggles in the highest of dimensions (10D), where other BO methods struggle as well. In the other benchmarks, SnAKE consistently achieves very good regret at low cost. The bounds are created from \pm half the standard deviation of all runs.

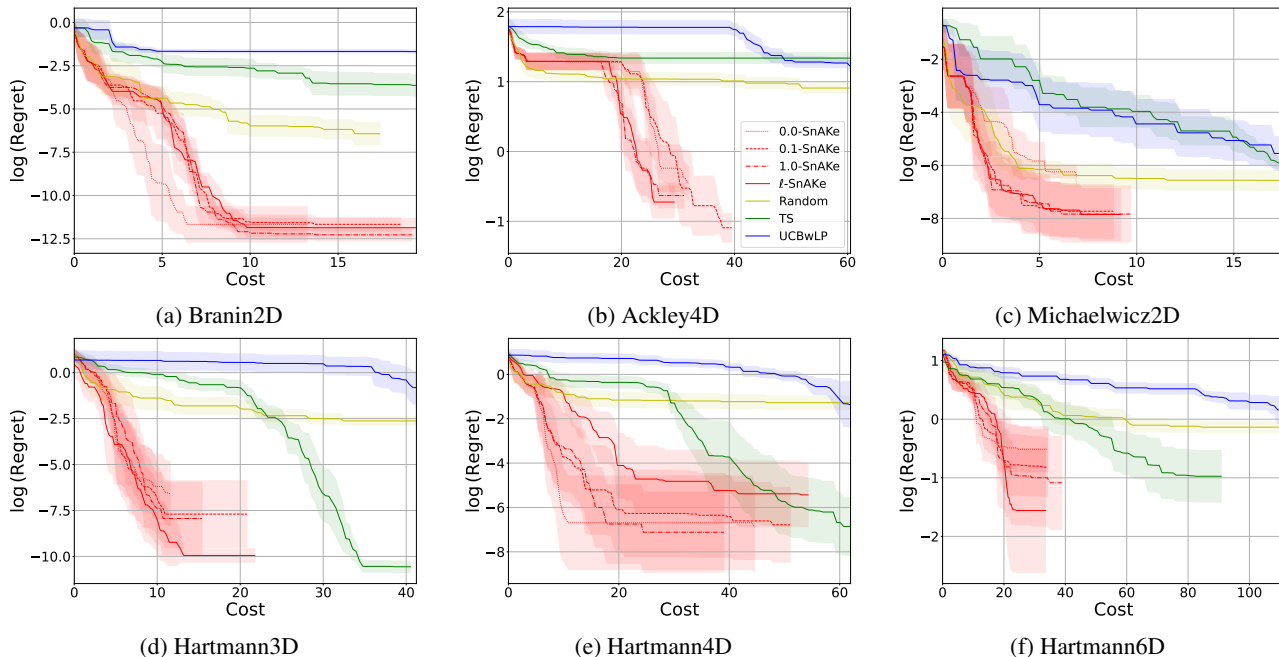


Figure 6. Results of synthetic experiments with $t_{\text{delay}} = 25$. We plot the average $\log(\text{regret})$ achieved against the cost spent. For every experiment we set $T = 250$, and limit the x -axis to the maximum cost achieved by SnAKE or Random. l -SnAKE is the non-parametric version of the algorithm. SnAKE consistently achieves very good regret against low cost. The bounds are created from \pm half the standard deviation of all runs.

Acknowledgements

JPF is funded by EPSRC through the Modern Statistics and Statistical Machine Learning (StatML) CDT (grant no. EP/S023151/1) and by BASF SE, Ludwigshafen am Rhein. SZ was supported by an Imperial College Hans Rausing PhD Scholarship. The research was funded by Engineering & Physical Sciences Research Council (EPSRC) Fellowships to RM and CT (grant no. EP/P016871/1 and EP/T001577/1). CT also acknowledges support from an Imperial College Research Fellowship.

Discussions with colleagues in the Imperial Department of Computing led to the ideas of ϵ -Point Deletion and the nonparametric ℓ -SnAKE. Linden Schrecker improved our understanding of the chemistry application.

References

- Alvi, A., Ru, B., Calliess, J.-P., Roberts, S., and Osborne, M. A. Asynchronous Batch Bayesian Optimisation with Improved Local Penalisation. In *Proceedings of the 36th International Conference on Machine Learning*, pp. 253–262, 09–15 Jun 2019.
- Azimi, J., Fern, A., and Fern, X. Z. Batch Bayesian Optimization via simulation matching. In *Advances in Neural Information Processing Systems*, pp. 109–117. Citeseer, 2010.
- Balandat, M., Karrer, B., Jiang, D. R., Daulton, S., Letham, B., Wilson, A. G., and Bakshy, E. BoTorch: A Framework for Efficient Monte-Carlo Bayesian Optimization. In *Advances in Neural Information Processing Systems 33*, 2020.
- Bellman, R. Dynamic Programming Treatment of the Travelling Salesman Problem. *Journal of the ACM (JACM)*, 9(1):61–63, 1962.
- Dorigo, M. and Gambardella, L. M. Ant colonies for the travelling salesman problem. *Biosystems*, 43(2):73–81, 1997.
- Fath, V., Lau, P., Greve, C., Weller, P., Kockmann, N., and Röder, T. Simultaneous self-optimisation of yield and purity through successive combination of inline FT-IR spectroscopy and online mass spectrometry in flow reactions. *Journal of Flow Chemistry*, 11(3):285–302, 2021.
- Felton, K., Rittig, J., and Lapkin, A. Summit: Benchmarking Machine Learning Methods for Reaction Optimisation. *Chemistry Methods*, February 2021.
- Gardner, J., Pleiss, G., Bindel, D., Weinberger, K., and Wilson, A. Gpytorch: Blackbox matrix-matrix Gaussian Process inference with GPU acceleration. *Advances in Neural Information Processing Systems*, pp. 7576–7586, 2018.
- Ginsbourger, D., Le Riche, R., and Carraro, L. Kriging is well-suited to Parallelize Optimization. In *Computational Intelligence in Expensive Optimization Problems*, Springer series in Evolutionary Learning and Optimization, pp. 131–162. 2010.
- González, J., Dai, Z., Hennig, P., and Lawrence, N. Batch Bayesian Optimization via Local Penalization. In *Proceedings of the 19th International Conference on Artificial Intelligence and Statistics*, pp. 648–657, 09–11 May 2016a.
- González, J., Osborne, M., and Lawrence, N. GLASSES: Relieving The Myopia Of Bayesian Optimisation. In *Proceedings of the 19th International Conference on Artificial Intelligence and Statistics*, pp. 790–799, 09–11 May 2016b.
- Hagberg, A., Swart, P., and S Chult, D. Exploring network structure, dynamics, and function using NetworkX. Technical report, Los Alamos National Lab. (LANL), 2008.
- Hone, C. A., Holmes, N., Akien, G. R., Bourne, R. A., and Muller, F. L. Rapid multistep kinetic model generation from transient flow data. *React. Chem. Eng.*, 2:103–108, 2017.
- Jiang, S., Chai, H., González, J., and Garnett, R. BINOCULARS for Efficient, Non-myopic Sequential Experimental Design. In *Proceedings of the 37th International Conference on Machine Learning*, pp. 4794–4803, 13–18 Jul 2020.
- Jones, D. R., Schonlau, M., and Welch, W. J. Efficient global optimization of expensive black-box functions. *Journal of Global optimization*, 13(4):455–492, 1998.
- Kandasamy, K., Krishnamurthy, A., Schneider, J., and Póczos, B. Parallelised Bayesian Optimisation via Thompson Sampling. In *Proceedings of the Twenty-First International Conference on Artificial Intelligence and Statistics*, pp. 133–142, 2018.
- Kandasamy, K., Dasarthy, G., Oliva, J., Schneider, J., and Póczos, B. Multi-fidelity Gaussian Process Bandit Optimisation. *Journal of Artificial Intelligence Research*, 66: 151–196, 2019.
- Kingma, D. and Ba, J. Adam: A Method for Stochastic Optimization. *International Conference on Learning Representations*, 12 2014.
- Kirkpatrick, S., Gelatt, C. D., and Vecchi, M. P. Optimization by simulated annealing. *Science*, 220(4598): 671–680, 1983.

- Kushner, H. J. A New Method of Locating the Maximum Point of an Arbitrary Multipeak Curve in the Presence of Noise. *Journal of Basic Engineering*, 86:97–106, 1964.
- Lam, R., Willcox, K., and Wolpert, D. H. Bayesian optimization with a finite budget: An approximate dynamic programming approach. *Advances in Neural Information Processing Systems*, 29:883–891, 2016.
- Lazzari, S., Lischewski, A., Orlov, Y., Deglmann, P., Daiss, A., Schreiner, E., and Vale, H. *Toward a digital polymer reaction engineering*, volume 56, pp. 187–227. 01 2020.
- McMullen, J. P. and Jensen, K. F. Rapid Determination of Reaction Kinetics with an Automated Microfluidic System. *Organic Process Research & Development*, 15 (2):398–407, 2011.
- Mockus, J., Tiesis, V., and Zilinskas, A. The application of Bayesian methods for seeking the extremum. *Towards Global Optimization*, 2:117–129, 09 2014.
- Paszke, A., Gross, S., Massa, F., Lerer, A., Bradbury, J., Chanan, G., Killeen, T., Lin, Z., Gimelshein, N., Antiga, L., Desmaison, A., Kopf, A., Yang, E., DeVito, Z., Raison, M., Tejani, A., Chilamkurthy, S., Steiner, B., Fang, L., Bai, J., and Chintala, S. PyTorch: An Imperative Style, High-Performance Deep Learning Library. In *Advances in Neural Information Processing Systems 32*, pp. 8024–8035. Curran Associates, Inc., 2019.
- Rasmussen, C. E. and Williams, C. K. I. *Gaussian Processes for Machine Learning (Adaptive Computation and Machine Learning)*. The MIT Press, 2005.
- Shahriari, B., Swersky, K., Wang, Z., Adams, R. P., and de Freitas, N. Taking the Human Out of the Loop: A Review of Bayesian Optimization. *Proceedings of the IEEE*, 104(1):148–175, 2016.
- Snelson, E. and Ghahramani, Z. Sparse Gaussian Processes Using Pseudo-Inputs. In *Advances in Neural Information Processing Systems*, pp. 1257–1264. MIT Press, 2005.
- Sobol’, I. M. On the distribution of points in a cube and the approximate evaluation of integrals. *Zhurnal Vychislitel’noi Matematiki i Matematicheskoi Fiziki*, 7(4): 784–802, 1967.
- Srinivas, N., Krause, A., Kakade, S., and Seeger, M. Gaussian Process Optimization in the Bandit Setting: No Regret and Experimental Design. In *Proceedings of the 27th International Conference on International Conference on Machine Learning*, pp. 1015–1022, 2010.
- Surjanovic, S. and Bingham, D. Virtual Library of Simulation Experiments: Test Functions and Datasets. Available at <http://www.sfu.ca/~ssurjano>, 2013.
- Teh, S.-Y., Lin, R., Hung, L.-H., and Lee, A. P. Droplet microfluidics. *Lab Chip*, 8:198–220, 2008.
- Vellanki, P., Rana, S., Gupta, S., Rubin, D., Sutti, A., Dorin, T., Height, M., Sanders, P., and Venkatesh, S. Process-constrained Batch Bayesian Optimisation. In *Advances in Neural Information Processing Systems*. Curran Associates, Inc., 2017.
- Waldron, C., Pankajakshan, A., Quaglio, M., Cao, E., Galvanin, F., and Gavriilidis, A. An autonomous microreactor platform for the rapid identification of kinetic models. *React. Chem. Eng.*, 4:1623–1636, 2019.
- Wilson, J., Borovitskiy, V., Terenin, A., Mostowsky, P., and Deisenroth, M. Efficiently Sampling Functions from Gaussian Process Posteriors. In *Proceedings of the 37th International Conference on Machine Learning*, pp. 10292–10302, 13-18 Jul 2020.
- Yue, X. and Kontar, R. A. Why Non-myopic Bayesian Optimization is Promising and How Far Should We Look-ahead? A Study via Rollout. In *Proceedings of the Twenty Third International Conference on Artificial Intelligence and Statistics*, pp. 2808–2818, 26–28 Aug 2020.

A. Empirical Analysis of Escape Probability

A.1. Areas with stationary points

Figure 7 estimates the non-escape probability (see Definition 3.2) from the interval $A = [0.1, 0.2]$. The optimization objective is a bi-modal function. Once we have 15 samples in the interval $[0.1, 0.2]$, we estimate the escape probability to converge to $p \approx 0.74$.

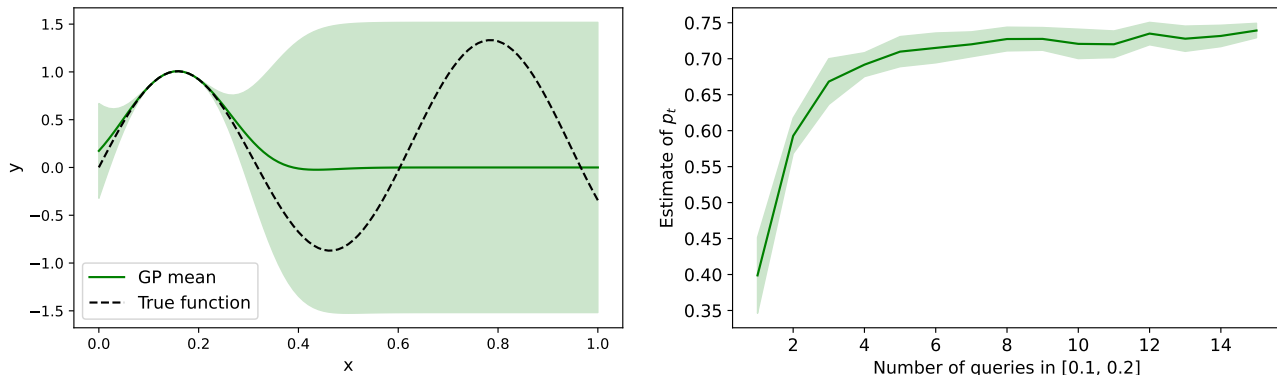


Figure 7. We estimate the probability of non-escape by taking 5000 independent Thompson Samples and counting the number of samples inside A (i.e. the MLE estimator of the Bernoulli distribution). We do this for increasing number of training points in A (which are chosen randomly with a uniform distribution in A). We repeat the experiment 10 times. The left plot shows the underlying function and the Gaussian Process for 15 training points. The right plot shows the evolution of our estimate as we increase training points inside $A = [0.1, 0.2]$ (we plot the mean of each run \pm the standard deviation). This example makes it clear that p_t does not converge to zero. Furthermore, it seems to converge to just over 0.7 which a very large probability. This will make fully escaping the local minimum very difficult without Point Deletion.

A.2. Areas without stationary points

We now repeat the same experiment as in section A.1, this time we change the interval to $A = [0.0, 0.1]$ which does not contain any stationary points. One can observe a clear difference in the behavior of p_t as we include more information. This time, $p_t \rightarrow 0$ very fast.

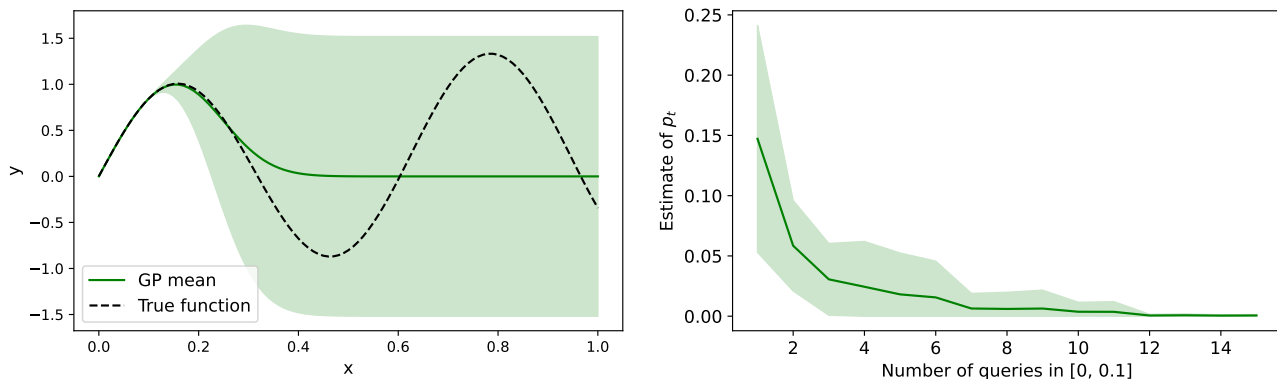


Figure 8. We estimate the probability of non-escape by taking 5000 independent Thompson Samples and counting the number of samples inside A (i.e. the MLE estimator of the Bernoulli distribution). We do this for increasing number of training points in A (which are chosen randomly with a uniform distribution in A). We repeat the experiment 10 times. The left plot shows the underlying function and the Gaussian Process for 15 training points. The right plot shows the evolution of our estimate as we increase training points inside $A = [0, 0.1]$ (we plot the mean of each run \pm the standard deviation). We can see that p_t quickly converges to (almost) zero. We almost guaranteed to fully escape the area after 15 time-steps, even for very large budgets.

A.3. Resampling vs Point Deletion

Figure 9 empirically confirms the analysis of Section 3.8 showing the effectiveness of ϵ -Point Deletion, and displaying the effect of increasing the budget from 100 to 250 iterations.

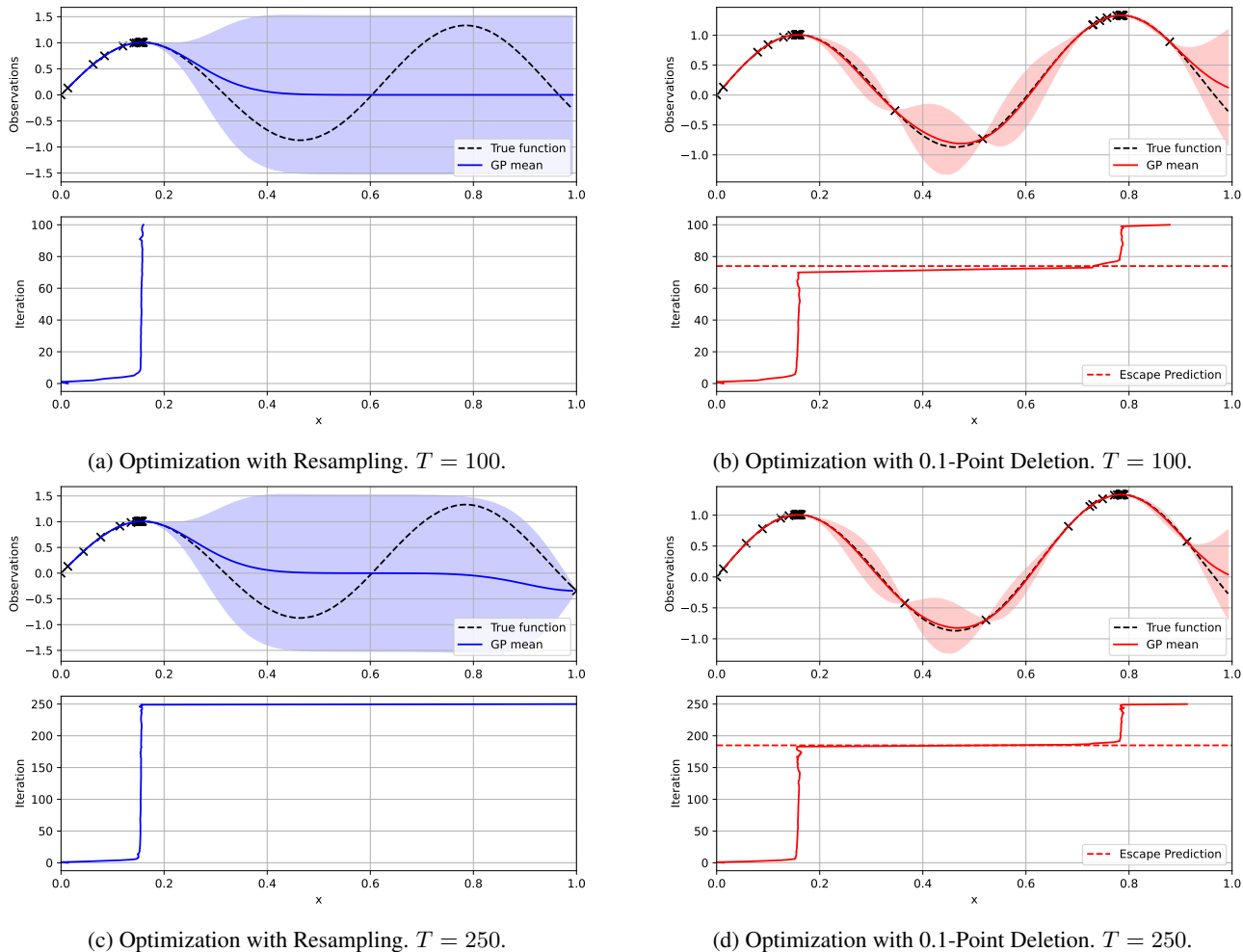


Figure 9. We investigate the effect of Point Deletion, and empirically confirm our analysis from Section 3.7. For Point Deletion, we calculate the escape prediction as pT , using $\hat{p} \approx 0.74$, which we estimated in Section A.1. We can see that without Point Deletion, the escape happens until *until the very last* iteration, independently of the budget (see Remark 3.4 for an explanation). With Point Deletion, we can see that our escape predictions are accurate, and the exploration of the actual optimum increases with the budget.

B. Implementation Details

This section outlines the implementation details and hyper-parameter choices for all the methods compared in the paper. The code will be made available open source after peer review.

B.1. Gaussian Processes

For every GP, we use the RBF Kernel with an output-scale, θ_0 :

$$k_{RBF}(x_1, x_2) = \theta_0 \exp\left(-\frac{1}{2}(x_1 - x_2)^T \Theta^{-2}(x_1 - x_2)\right)$$

where $\Theta = \text{diag}(\ell_1, \dots, \ell_d)$ and ℓ_i denotes the length-scale of the i th variable. For the prior mean, we used a constant function with trainable value, μ_0 . We implemented them all using the package GPyTorch (Gardner et al., 2018).

B.2. Training the hyper-parameters of the Gaussian Processes

Our method is well suited for physical systems. Hence, we assume that there is good prior knowledge of the hyper-parameters. In particular, we found it reasonable that each hyper-parameter would be given a lower and upper bound. Normally, we would simply have a large initialization sample. However, we believe this goes against the nature of the problem because we want to explore the space slowly to avoid large input costs. So any type of initialization would be costly.

We simulate this in the following way: we first randomly sample $\max(T/5, 10d)$ points from the d -dimensional input space, and train a GP on these data-points. The hyper-parameters of the GP are optimized by maximizing the marginal log-likelihood (Rasmussen & Williams, 2005) over 500 epochs using Adam (Kingma & Ba, 2014) with a learning rate of 0.01. The resulting hyper-parameters will correspond to the ‘educated guess’. We then set the following bounds:

- a) For the length-scale, the lower bound is half the educated guess, and the upper bound double the ‘educated guess’.
- b) For the output-scale, θ_0 , the lower bound is half the educated guess, and the upper bound double the ‘educated guess’.
- c) For the initial mean, μ_0 , the lower bound is the educated guess minus a third of the initial variance, the upper bound is the educated guess plus a third of the initial variance.
- d) The noise parameter we simply set to be greater than 10^{-5} .

We (partially) enforce the constraints by setting a SmoothedBoxPrior on each parameter, with a variance of 0.001. Finally, under the constraints defined above, we re-estimate the hyper-parameters every time we obtain 25 new observations.

To make sure all models receive fair initializations, we set the same seed for each run and function pair.

B.3. SnAKe

We used Simulated Annealing (Kirkpatrick et al., 1983) to solve the Travelling Salesman Problem. We implemented it using the NetworkX package (Hagberg et al., 2008). We initialized the cycle with the ‘greedy’ sub-algorithm and used all default options.

We generated the Thompson Samples using the method introduced in Wilson et al. (2020) which we implemented ourselves. To optimize the samples we used Adam (Kingma & Ba, 2014) and PyTorch (Paszke et al., 2019) over $10d$ epochs, with a learning rate of 0.01. We used $10d$ multi-starts for each sample. To create the samples, we used $\ell = 1024$ Fourier bases.

For ℓ -SnAKe, we define an adaptive deletion constant, $\epsilon_t = \min(\ell_{1,t}, \dots, \ell_{d,t})$, where $\ell_{i,t}$ denotes the length scale of the i th variable at time t (recall we are re-training the hyper-parameters every new 25 observations, so the length scales change with time).

For the adaptive grid, we use $N_l = 25$ local samples, and a coarse global Sobol grid (Sobol’, 1967) of $N_g = 100$ points.

B.4. Classical Bayesian Optimization

We used BoTorch (Balandat et al., 2020) to implement all methods in this section. We optimized the acquisition functions across 150 epochs using Adam (Kingma & Ba, 2014) with a learning rate of 0.0001 using 7500 random multi-starts.

B.4.1. EXPECTED IMPROVEMENT

Expected Improvement (Mockus et al., 2014) optimizes the acquisition function:

$$EI(x) = \mathbb{E} [\max(y - y_{best}, 0)], \quad y \sim f(x)$$

where y_{best} is our best observation so far.

B.4.2. UPPER CONFIDENCE BOUND

Upper Confidence Bound (Srinivas et al., 2010) optimizes the acquisition function:

$$UCB(x) = \mu_t(x) + \beta_t \sigma_t(x)$$

We set $\beta_t = 0.2d \log(2t)$ following Kandasamy et al. (2019).

B.4.3. PROBABILITY OF IMPROVEMENT

Probability of Improvement (Kushner, 1964) optimizes the acquisition function:

$$PI(x) = \mathbb{P}(y \geq y_{best}), \quad y \sim f(x)$$

B.5. Asynchronous Bayesian Optimization

B.5.1. UCB WITH LOCAL PENALIZATION

We use the method as is described in González et al. (2016a). We set $\beta_t = 0.2d \log(2t)$ and $M = y_{best}$. For the Lipschitz constant, we estimate it by calculating the gradient of μ_t (using auto-differentiation) in a Sobol grid (Sobol', 1967) of $50d$ points and selecting L to be the maximum gradient in the grid.

B.5.2. THOMPSON SAMPLING

We use the sample procedure as in B.3, except we only optimize a single sample at every iteration.

B.6. Description of Benchmark Functions

We chose the benchmark functions to observe the behavior of SnAKE in a variety of scenarios. More details of all the benchmark functions can be found in Surjanovic & Bingham (2013).

B.6.1. BRANIN2D

The two-dimensional Branin function is given by. The function has three global maximums:

$$f(x) = a(x_2 - bx_1^2 + cx_1 - r)^2 + s(1 - t) \cos(x_1) + s$$

where we optimize over $\mathcal{X} = [-5, 10] \times [0, 15]$. We set $a = -1$, $b = 5.1/(4\pi^2)$, $c = 5/\pi$, $r = 6$, $s = -10$, and $t = 1/(8\pi)$.

B.6.2. ACKLEY4D

The four-dimensional Ackley function has a lot of local optimums, with the optima in the center of the search space. The function is given by:

$$f(x) = a \exp \left(-b \sqrt{\frac{1}{4} \sum_{i=1}^4 x_i^2} \right) + \exp \left(\frac{1}{d} \sum_{i=1}^4 \cos(cx_i) \right) - a - \exp(1)$$

where we slightly shift the search space and optimize over $\mathcal{X} = [-1.8, 2.2]^4$. This is to avoid having the optimum exactly at a point in the Sobol grid and giving SnAKE an unfair advantage. We set $a = 20$, $b = 0.2$, and $c = 2\pi$.

B.6.3. MICHAELWICZ2D

The two-dimensional Michalewicz function is characterized by multiple local maxima and a lot of flat regions. The function is given by:

$$f(x) = \sum_{i=1}^2 \sin(x_i) \sin^{2m} \left(\frac{ix_i^2}{\pi} \right)$$

where we set $m = 10$ and we optimize on the region $\mathcal{X} = [0, \pi]^2$.

B.6.4. HARTMANN

We select this function to see how the algorithms behave in *similar* functions as dimension increases. We do three versions of the Hartmann function, with dimensions $d = 3, 4$, and 6 . The equation is given by:

$$f(x) = \sum_{i=1}^4 \alpha_i \exp \left(- \sum_{j=1}^d A_{ij} (x_j - P_{ij}) \right)$$

where $\alpha = (1, 1.2, 3, 3.2)^T$. For $d = 3$ we use:

$$A = \begin{pmatrix} 3 & 10 & 30 \\ 0.1 & 10 & 35 \\ 3 & 10 & 30 \\ 0.1 & 10 & 35 \end{pmatrix} \quad P = 10^{-4} \begin{pmatrix} 3689 & 1170 & 2673 \\ 4699 & 4387 & 7470 \\ 1091 & 8732 & 5547 \\ 381 & 5743 & 8828 \end{pmatrix}$$

for $d = 4$ and $d = 6$ we use:

$$A = \begin{pmatrix} 10 & 3 & 17 & 3.5 & 1.7 & 8 \\ 0.05 & 10 & 17 & 0.1 & 8 & 14 \\ 3 & 3.5 & 1.7 & 10 & 17 & 8 \\ 17 & 8 & 0.05 & 10 & 0.1 & 14 \end{pmatrix} \quad P = 10^{-4} \begin{pmatrix} 1312 & 1696 & 5569 & 124 & 8283 & 5886 \\ 2329 & 4135 & 8307 & 3736 & 1004 & 9991 \\ 2348 & 1451 & 3522 & 2883 & 3047 & 6650 \\ 4047 & 8828 & 8732 & 5743 & 1091 & 381 \end{pmatrix}$$

They are all evaluated on the unit cube $[0, 1]^d$.

B.6.5. PERM10D

We select the 10-dimensional version of the Perm benchmark to test the capabilities of the algorithms in a very high-dimensional setting (by BO standards). The equation is given by:

$$f(x) = -10^{-21} \sum_{i=1}^{10} \left(\sum_{j=1}^{10} (j^i + \beta) \left(\left(\frac{x_j}{j} \right)^i - 1 \right) \right)^2$$

where we set $\beta = 10$. We evaluate it on $\mathcal{X} = [-10, 10]^d$.

B.6.6. SNAR 3D

Since the SnAr benchmark is a multi-objective problem, we optimize a weighted sum of the two objectives:

$$\text{SnAr}(x) = \omega_1 \times \text{yield} - \omega_2 \times \text{e-factor}$$

where we set $\omega_1 = 10^{-4}$ and $\omega_2 = 0.2$. We optimize over $\mathcal{X} = [40, 120] \times [0.1, 0.5] \times [1, 5]$. For simplicity, we fix the residence time to 1.

C. Full Experiment Results

C.1. Tables of Results

C.1.1. SYNCHRONOUS EXPERIMENTS

This section includes the full tables of results of the synthetic synchronous experiments. The results are shown in Table 1 and 2.

C.1.2. ASYNCHRONOUS EXPERIMENTS

In this section we include the full table results of all asynchronous experiments. The results are shown in Table 3 and 4.

C.1.3. SNAR BENCHMARK

We ran additional experiments on the SnAr benchmark. For the first one (which includes the example looked at in the main paper) we tested on a budget of $T = 100$ iterations for different values of t_{delay} . The results are included in Tables 5 and 6.

We also carried out synchronous results on the benchmark, for different budgets. The results are included in Tables 7 and 8.

C.2. Graphs for results of Section 4.1.1

We include the full graphs of the sequential Bayesian Optimization experiments. Each row represents a different budget. The left column shows the evolution of regret against the cost used, the middle column shows the evolution of regret with

Table 1. Comparison of 2-norm cost for different BO benchmark functions. The best three performances are shown in bold, and the best one in italics. We can see that SnAKE constantly achieves the lowest cost, especially for larger budgets. The best cost performance is achieved by 0.0-SnAKE, however, we do this at the expense of worse regret. The only function for which SnAKE struggles is the very high dimensional Perm10D.

Method	Budget	0.0-SnAKE	0.1-SnAKE	1.0-SnAKE	ℓ -SnAKE	EI	UCB	PI	Random
Branin2D	15	4.8 ± 2.3	5.0 ± 2.3	5.4 ± 2.1	5.2 ± 1.9	7.1 ± 1.4	5.1 ± 1.4	1.0 ± 0.9	4.23 ± 0.18
	50	6.2 ± 3.5	9 ± 4	8 ± 4	8.8 ± 3.5	17 ± 5	18 ± 5	5 ± 4	7.31 ± 0.33
	100	5.4 ± 2.6	10 ± 5	9 ± 4	10 ± 4	35 ± 11	41 ± 10	15 ± 7	10.2 ± 0.5
	250	7.1 ± 1.9	15.2 ± 3.3	15 ± 5	15.5 ± 3.5	110 ± 35	115 ± 21	37 ± 21	16.3 ± 0.6
Ackley4D	15	14.8 ± 1.2	15.0 ± 1.1	15.6 ± 0.8	16.2 ± 0.5	20.6 ± 0.7	17.1 ± 0.7	14.5 ± 1.0	7.96 ± 0.30
	50	24 ± 5	26 ± 4	29 ± 4	26 ± 4	62 ± 8	50 ± 4	42.6 ± 2.6	19.5 ± 0.7
	100	24 ± 5	29 ± 8	25 ± 7	25 ± 4	119 ± 7	92 ± 7	82.1 ± 3.0	32.9 ± 0.8
	250	25 ± 7	34 ± 9	31 ± 7	34.2 ± 3.5	278 ± 19	195 ± 19	200 ± 4	60.2 ± 1.1
Michaelwicz2D	15	1.6 ± 0.7	1.7 ± 0.6	1.7 ± 0.8	2.0 ± 0.8	12.0 ± 2.7	6.5 ± 1.8	5 ± 5	3.91 ± 0.29
	50	2.1 ± 0.5	3.1 ± 0.8	2.9 ± 0.9	3.4 ± 1.0	23 ± 6	18.6 ± 2.0	12 ± 18	7.56 ± 0.31
	100	2.2 ± 0.6	4.1 ± 0.9	3.6 ± 0.8	3.9 ± 1.0	30 ± 13	35.3 ± 3.3	25 ± 33	10.5 ± 0.4
	250	2.4 ± 0.7	5.2 ± 1.5	4.5 ± 1.3	5.5 ± 0.9	(5 ± 4) × 10 ¹	83 ± 12	(7 ± 5) × 10 ¹	16.57 ± 0.35
Hartmann3D	15	2.1 ± 1.1	3.1 ± 0.7	3.8 ± 1.3	3.4 ± 0.9	7.3 ± 3.2	5.7 ± 1.4	4 ± 4	6.37 ± 0.22
	50	5.4 ± 2.6	5.6 ± 2.6	8 ± 4	6.3 ± 3.3	14.0 ± 2.2	19.0 ± 1.9	8 ± 4	13.8 ± 0.5
	100	6.7 ± 3.0	11 ± 5	10 ± 4	11 ± 5	46 ± 10	37.6 ± 3.5	19 ± 11	21.5 ± 0.6
	250	5.7 ± 2.9	11 ± 4	10 ± 4	10 ± 4	97 ± 6	90 ± 4	(6 ± 5) × 10 ¹	38.4 ± 1.1
Hartmann6D	15	7 ± 4	7.6 ± 3.5	8 ± 4	8 ± 4	19 ± 4	14.4 ± 2.0	16 ± 7	10.5 ± 0.5
	50	12 ± 5	11 ± 4	14 ± 7	12.4 ± 3.3	63 ± 13	49 ± 6	38 ± 17	29.5 ± 0.9
	100	12 ± 4	14 ± 5	16 ± 10	11 ± 5	112 ± 30	97 ± 4	69 ± 32	51.6 ± 1.0
	250	14 ± 6	15 ± 6	18 ± 8	14 ± 5	(2.8 ± 0.7) × 10 ²	239 ± 16	(1.7 ± 0.8) × 10 ²	108.0 ± 1.6
Perm10D	15	22.1 ± 0.9	22.1 ± 0.9	22.5 ± 0.9	21.9 ± 1.3	26.1 ± 2.2	18.3 ± 0.9	16 ± 6	14.98 ± 0.29
	50	66.3 ± 3.4	66.2 ± 3.0	67.8 ± 2.3	67.1 ± 3.3	98 ± 5	67.9 ± 2.3	43 ± 20	45.2 ± 0.8
	100	119 ± 4	117 ± 4	129 ± 12	118 ± 5	201 ± 7	141.0 ± 3.2	(8 ± 4) × 10 ¹	82.7 ± 0.9
	250	255 ± 14	256 ± 12	281 ± 9	250 ± 6	493 ± 16	363 ± 7	(2.1 ± 1.1) × 10 ²	183.3 ± 1.2

iterations, and the right column shows the evolution of the 2-norm cost. The results encompass Figures 10 to 15. The caption in each figure tells us the benchmark function being evaluated. Each experiment is the mean ± half the standard deviation of 10 different runs.

C.3. Graphs for results of Section 4.1.2

We include the full graphs of the asynchronous Bayesian Optimization experiments. Each row represents a different budget. The left column shows the evolution of regret against the cost used, the middle column shows the evolution of regret with iterations, and the right columns show the evolution of the 2-norm cost. The results encompass Figures 16 to 27. The caption in each figure tells us the benchmark function being evaluated, and the time-delay for getting observations back. Each experiment is the mean ± half the standard deviation of 10 different runs.

C.4. Graphs for results of SnAr Benchmark (section 4.2)

Figure 28 includes the whole set of results of the SnAr benchmark in the asynchronous setting. Figure 29 includes the results for the synchronous setting. Each experiment is the mean ± half the standard deviation of 10 different runs.

SnAKE: Bayesian Optimization with Pathwise Exploration

Table 2. Comparison of final log(regret) for different BO benchmark functions. The best three performances are shown in bold, and the best one in italics. We can see that SnAKE constantly achieves regret comparable with classical Bayesian Optimization methods. The worst performance happens when $\epsilon = 0$, this could be explained by the method getting stuck in local optimums.

Method	Budget	0.0-SnAKE	0.1-SnAKE	1.0-SnAKE	ℓ -SnAKE	EI	UCB	PI	Random
Branin2D	15	-3.9 ± 1.3	-3.4 ± 0.9	-3.6 ± 1.0	-3.4 ± 0.9	-5.1 ± 1.8	-5.4 ± 1.1	-3.5 ± 1.2	-3.2 ± 0.6
	50	-6.2 ± 2.8	-8 ± 4	-7.2 ± 3.1	-7.7 ± 2.9	-8.7 ± 1.7	-7.4 ± 1.1	-6.1 ± 2.2	-4.4 ± 0.9
	100	-8.9 ± 3.2	-11.1 ± 2.7	-11.5 ± 3.3	-10.8 ± 2.7	-11.9 ± 2.1	-8.4 ± 0.8	-10.7 ± 1.4	-5.2 ± 1.1
	250	-11.8 ± 1.3	-13.0 ± 1.1	-13.9 ± 1.4	-13.7 ± 1.7	-15 ± 7	-10.4 ± 1.7	-11.1 ± 1.2	-6.0 ± 0.7
Ackley4D	15	1.5 ± 0.4	1.5 ± 0.4	1.5 ± 0.4	1.67 ± 0.25	1.70 ± 0.14	1.70 ± 0.14	1.40 ± 0.14	1.45 ± 0.07
	50	1.72 ± 0.14	1.71 ± 0.12	1.71 ± 0.13	1.74 ± 0.11	1.39 ± 0.15	1.66 ± 0.11	1.21 ± 0.10	1.18 ± 0.18
	100	1.66 ± 0.19	1.66 ± 0.19	1.66 ± 0.19	1.72 ± 0.11	1.25 ± 0.11	1.66 ± 0.11	1.16 ± 0.10	1.03 ± 0.18
	250	1.50 ± 0.19	0.8 ± 0.8	1.34 ± 0.23	1.0 ± 0.4	1.11 ± 0.13	1.2 ± 0.5	1.00 ± 0.07	0.84 ± 0.21
Michaelwicz2D	15	-3.9 ± 1.8	-4.7 ± 1.2	-5.4 ± 2.0	-4.0 ± 1.8	-5.3 ± 1.6	-5.8 ± 1.8	-4.1 ± 1.8	-4.1 ± 1.0
	50	-6.7 ± 1.8	-7.4 ± 1.4	-6.9 ± 1.2	-6.5 ± 2.0	-5.6 ± 1.8	-8.8 ± 2.3	-6.2 ± 2.5	-5.4 ± 0.4
	100	-6.5 ± 1.0	-6.8 ± 1.1	-7.4 ± 1.6	-7.5 ± 2.0	-5.9 ± 0.8	-9.8 ± 2.0	-6.7 ± 2.8	-6.1 ± 0.4
	250	-6.4 ± 0.8	-7.5 ± 1.3	-8.1 ± 1.8	-8.0 ± 2.0	-6.1 ± 0.5	-11.1 ± 2.0	-7.2 ± 1.9	-6.3 ± 0.6
Hartmann3D	15	-1.0 ± 1.4	-2.3 ± 2.0	-1.7 ± 2.1	-1.6 ± 1.6	-1.9 ± 1.7	-2.0 ± 1.2	-0.4 ± 0.9	-0.3 ± 0.8
	50	-2.6 ± 2.0	-4.0 ± 2.8	-3.9 ± 2.2	-3.9 ± 2.2	-6.7 ± 1.6	-3.8 ± 0.7	-4.5 ± 2.2	-1.3 ± 0.5
	100	-4.9 ± 2.0	-8.2 ± 1.3	-8.1 ± 1.2	-8.3 ± 0.8	-10.0 ± 1.0	-4.4 ± 0.6	-7.5 ± 1.6	-1.5 ± 0.5
	250	-5 ± 4	-8.6 ± 3.4	-8.6 ± 3.0	-8.5 ± 2.9	-10.6 ± 1.7	-5.3 ± 0.8	-10.0 ± 1.4	-2.6 ± 0.6
Hartmann6D	15	0.77 ± 0.31	0.76 ± 0.33	0.65 ± 0.30	0.6 ± 0.4	0.83 ± 0.35	0.59 ± 0.27	0.8 ± 0.5	0.62 ± 0.34
	50	0.5 ± 0.5	0.0 ± 0.8	0.0 ± 0.9	0.1 ± 0.5	0.6 ± 0.5	0.2 ± 0.4	0.4 ± 0.8	0.56 ± 0.29
	100	0.1 ± 0.6	-0.1 ± 1.0	0.1 ± 0.9	-0.6 ± 0.8	-0.1 ± 0.9	-0.26 ± 0.35	-0.1 ± 0.8	0.21 ± 0.30
	250	-0.5 ± 0.9	-0.5 ± 0.8	-0.6 ± 1.0	-0.8 ± 1.1	-0.5 ± 1.0	-1.0 ± 0.6	-0.8 ± 1.0	0.05 ± 0.27
Perm10D	15	-2.1 ± 1.9	-2.1 ± 1.9	-2.1 ± 1.9	-2.8 ± 1.8	-4.1 ± 1.5	-6.3 ± 1.8	-6.0 ± 2.6	-5.4 ± 1.2
	50	-3.3 ± 1.7	-3.3 ± 1.7	-3.7 ± 1.7	-3.6 ± 1.3	-4.3 ± 1.7	-8.3 ± 2.1	-6.8 ± 2.4	-7.9 ± 1.8
	100	-3.2 ± 1.5	-3.2 ± 1.5	-4.5 ± 1.2	-4.0 ± 1.1	-4.3 ± 1.7	-9.3 ± 1.7	-8.0 ± 2.0	-8.0 ± 1.2
	250	-5.4 ± 2.4	-5.4 ± 2.4	-5.7 ± 2.3	-3.1 ± 1.5	-4.4 ± 1.5	-10.2 ± 1.5	-8.6 ± 2.0	-9.8 ± 1.6

Table 3. Comparison of 2-norm cost for different benchmark functions in the *asynchronous setting*. The best three performances are shown in bold, and the best one in italics. SnAKE achieves considerable lower cost with respect to other methods, achieving the top 3 lowest costs each time.

Method	Budget	Delay	0.0-SnAKE	0.1-SnAKE	1.0-SnAKE	ℓ -SnAKE	Random	TS	UCBwLP
Branin2D	100	10	6.5 ± 2.0	10.0 ± 2.9	10 ± 4	9.4 ± 3.5	10.4 ± 0.5	49 ± 5	26.4 ± 2.4
	100	25	7.8 ± 2.1	10.3 ± 3.1	7.9 ± 1.1	10.2 ± 3.1	10.3 ± 0.6	54 ± 5	49.4 ± 3.2
	250	10	7.8 ± 2.0	14.4 ± 1.9	16 ± 4	15.1 ± 2.1	16.6 ± 0.5	118 ± 12	37 ± 5
	250	25	9.3 ± 2.2	14.0 ± 1.7	14.2 ± 3.1	12.8 ± 3.2	16.8 ± 0.6	125 ± 10	54 ± 4
Ackley4D	100	10	22.3 ± 2.8	23.5 ± 1.7	21.7 ± 1.7	22.1 ± 2.1	32.3 ± 0.5	113 ± 5	98 ± 9
	100	25	18.9 ± 1.6	23.8 ± 1.9	24 ± 4	24 ± 4	32.6 ± 0.8	104 ± 9	100 ± 4
	250	10	27.5 ± 3.0	30.3 ± 2.9	26.1 ± 1.8	26.3 ± 1.4	59.2 ± 0.8	229 ± 17	256 ± 27
	250	25	27.5 ± 2.1	32.5 ± 3.3	25.9 ± 2.6	25.7 ± 2.2	59.6 ± 0.6	(2.2 ± 0.4) × 10 ²	239 ± 15
Michaelwicz2D	100	10	4.1 ± 1.7	5.9 ± 1.7	4.8 ± 1.0	5.0 ± 1.1	10.4 ± 0.5	18.8 ± 1.9	22.5 ± 1.7
	100	25	4.6 ± 1.1	6.2 ± 1.5	5.9 ± 1.3	6.3 ± 1.2	10.5 ± 0.4	26.6 ± 2.0	34.0 ± 2.9
	250	10	3.9 ± 2.1	5.7 ± 0.9	5.5 ± 1.5	6.2 ± 1.3	16.6 ± 0.6	28.1 ± 3.4	34.9 ± 3.3
	250	25	4.0 ± 1.3	6.7 ± 0.9	7.0 ± 1.2	7.0 ± 1.1	16.5 ± 0.7	36.0 ± 2.3	36.3 ± 2.7
Hartmann3D	100	10	8.9 ± 3.5	11 ± 5	9.8 ± 3.5	9 ± 5	21.8 ± 0.5	20.2 ± 3.2	35 ± 7
	100	25	10 ± 4	12.1 ± 3.1	13 ± 4	13 ± 4	21.3 ± 0.4	31.4 ± 2.3	54 ± 6
	250	10	6.2 ± 1.9	9.4 ± 2.8	9.4 ± 2.9	10.8 ± 2.6	38.7 ± 0.6	26 ± 4	44 ± 6
	250	25	7.0 ± 2.3	10 ± 4	9.8 ± 2.7	12 ± 4	38.8 ± 1.0	36.9 ± 2.8	63 ± 10
Hartmann4D	100	10	11 ± 5	16 ± 5	17 ± 5	24 ± 9	32.9 ± 0.5	38 ± 12	58 ± 10
	100	25	14.8 ± 3.2	20.1 ± 3.2	18 ± 4	24.0 ± 3.2	32.6 ± 0.9	43 ± 9	76 ± 10
	250	10	12 ± 7	21 ± 11	21 ± 8	23 ± 13	59.2 ± 0.8	(7 ± 4) × 10 ¹	103 ± 28
	250	25	16 ± 11	30 ± 15	22 ± 9	34 ± 14	59.5 ± 1.3	(9 ± 4) × 10 ¹	113 ± 22
Hartmann6D	100	10	15.0 ± 2.5	17 ± 4	19.5 ± 2.1	17.7 ± 3.4	51.5 ± 1.2	38 ± 9	116 ± 20
	100	25	21.5 ± 2.2	23.1 ± 1.8	25.0 ± 2.7	24 ± 4	51.7 ± 1.0	55 ± 7	111 ± 10
	250	10	18 ± 5	18 ± 5	19 ± 4	20 ± 8	106.6 ± 1.4	55 ± 21	(2.7 ± 0.6) × 10 ²
	250	25	21 ± 6	23 ± 6	23 ± 6	23 ± 5	106.6 ± 2.1	73 ± 12	(2.7 ± 0.4) × 10 ²

SnAKe: Bayesian Optimization with Pathwise Exploration

Table 4. Comparison of $\log(\text{regret})$ for different benchmark functions in the *asynchronous setting*. The best three performances are shown in bold, and the best one in italics. SnAKe achieves regret comparable with other Bayesian Optimization methods.

Method	Budget	Delay	0.0-SnAKe	0.1-SnAKe	1.0-SnAKe	ℓ -SnAKe	Random	TS	UCBwLP
Branin2D	100	10	-9.3 ± 2.7	-9.9 ± 2.6	-9.8 ± 2.7	-9.9 ± 2.8	-6.0 ± 2.7	-11.6 ± 1.1	-12.4 ± 1.7
	100	25	-6.4 ± 2.9	-7.2 ± 2.6	-6.3 ± 2.4	-6.4 ± 2.4	-5.1 ± 1.0	-11.8 ± 1.7	-7.7 ± 1.6
	250	10	-11.9 ± 2.2	-13.1 ± 0.5	-13.3 ± 1.2	-13.5 ± 1.0	-5.5 ± 0.4	-13.5 ± 1.1	-14.6 ± 1.4
	250	25	-11.7 ± 2.1	-11.7 ± 0.8	-12.3 ± 0.7	-11.9 ± 1.1	-6.4 ± 1.3	-13.7 ± 1.0	-15.2 ± 1.3
Ackley4D	100	10	1.2 ± 0.5	1.0 ± 0.6	1.1 ± 0.7	1.1 ± 0.7	1.11 ± 0.09	1.44 ± 0.16	1.14 ± 0.17
	100	25	1.23 ± 0.20	1.1 ± 0.5	1.14 ± 0.34	1.20 ± 0.28	1.10 ± 0.11	1.34 ± 0.16	1.02 ± 0.28
	250	10	-0.5 ± 0.8	-0.4 ± 1.0	-0.0 ± 0.7	-0.4 ± 0.4	0.85 ± 0.29	0.8 ± 0.7	0.2 ± 0.8
	250	25	-0.5 ± 0.5	-1.1 ± 0.4	-0.63 ± 0.35	-0.7 ± 0.5	0.91 ± 0.14	0.7 ± 0.6	0.82 ± 0.21
Michaelwicz2D	100	10	-7.0 ± 1.3	-7.1 ± 1.5	-7.0 ± 1.3	-7.6 ± 1.8	-6.2 ± 0.7	-7.2 ± 1.7	-8.9 ± 1.2
	100	25	-6.9 ± 1.7	-7.1 ± 2.0	-6.8 ± 0.9	-6.7 ± 1.1	-5.88 ± 0.19	-7.0 ± 1.0	-11.0 ± 1.8
	250	10	-6.4 ± 0.8	-7.6 ± 1.7	-8.0 ± 2.1	-7.7 ± 2.3	-6.5 ± 0.5	-8.0 ± 2.9	-8.9 ± 1.2
	250	25	-6.4 ± 0.6	-7.7 ± 2.0	-7.8 ± 2.1	-7.9 ± 1.9	-6.6 ± 0.8	-7.7 ± 2.2	-11.0 ± 1.8
Hartmann3D	100	10	-5.5 ± 3.1	-7.0 ± 3.2	-6 ± 4	-7.4 ± 2.8	-1.6 ± 0.5	-9.9 ± 1.3	-9.6 ± 1.0
	100	25	-5.5 ± 2.1	-6.4 ± 1.7	-5.6 ± 1.6	-7.3 ± 1.3	-1.6 ± 0.7	-9.3 ± 1.3	-6.5 ± 1.1
	250	10	-6 ± 4	-8.5 ± 2.9	-8 ± 4	-10.2 ± 0.7	-2.5 ± 0.6	-11.3 ± 0.9	-12.4 ± 0.9
	250	25	-6.6 ± 3.5	-8 ± 4	-8 ± 4	-9.9 ± 0.7	-2.6 ± 0.5	-10.6 ± 0.6	-12.3 ± 0.9
Hartmann4D	100	10	-3.6 ± 3.0	-3.4 ± 2.8	-3.8 ± 2.8	-2.1 ± 1.6	-1.3 ± 0.6	-6.3 ± 2.6	-3.8 ± 1.5
	100	25	-1.9 ± 1.7	-2.2 ± 2.1	-2.4 ± 2.6	-1.7 ± 1.0	-1.0 ± 0.6	-4.1 ± 1.4	-1.4 ± 0.8
	250	10	-7 ± 4	-6 ± 4	-6 ± 4	-4.0 ± 3.2	-1.1 ± 0.4	-8.2 ± 2.4	-7.0 ± 1.2
	250	25	-7 ± 4	-6.8 ± 3.4	-7 ± 4	-5.4 ± 2.9	-1.3 ± 0.6	-8.8 ± 1.3	-5.9 ± 1.9
Hartmann6D	100	10	-0.3 ± 0.6	-0.4 ± 0.9	-0.4 ± 0.7	-0.3 ± 1.3	0.1 ± 0.5	-0.3 ± 0.9	0.1 ± 0.8
	100	25	-0.4 ± 0.4	-0.4 ± 0.4	-0.4 ± 0.6	-0.2 ± 0.6	0.09 ± 0.31	-0.5 ± 0.6	0.22 ± 0.30
	250	10	-0.5 ± 1.0	-1.1 ± 1.2	-0.8 ± 0.8	-1.1 ± 2.3	-0.2 ± 0.6	-0.8 ± 1.0	-1.4 ± 0.6
	250	25	-0.5 ± 0.8	-0.8 ± 1.0	-1.1 ± 1.6	-1.6 ± 2.1	-0.14 ± 0.20	-1.0 ± 0.9	-0.9 ± 0.6

Table 5. Comparison of cost on SnAr benchmark (asynchronous) for $T = 100$ and different values of t_{delay} . The best three performances are shown in bold, and the best one in italics. SnAKe consistently achieves lower cost than BO methods.

delay	0.0-SnAKe	0.1-SnAKe	1.0-SnAKe	ℓ -SnAKe	Random	TS	UCBwLP
5	338 ± 31	378 ± 35	$(3.9 \pm 0.4) \times 10^2$	398 ± 32	361 ± 13	$(9.5 \pm 0.9) \times 10^2$	$(9.1 \pm 0.9) \times 10^2$
10	$(2.9 \pm 0.4) \times 10^2$	365 ± 34	$(3.0 \pm 0.4) \times 10^2$	361 ± 18	354 ± 14	$(1.04 \pm 0.06) \times 10^3$	$(8.7 \pm 0.8) \times 10^2$
25	$(2.6 \pm 0.4) \times 10^2$	$(3.2 \pm 0.4) \times 10^2$	$(3.0 \pm 0.5) \times 10^2$	$(3.5 \pm 0.5) \times 10^2$	355 ± 13	$(1.00 \pm 0.04) \times 10^3$	$(9.9 \pm 0.8) \times 10^2$
50	248 ± 32	308 ± 31	247 ± 24	$(3.1 \pm 0.4) \times 10^2$	359 ± 15	$(1.04 \pm 0.04) \times 10^3$	$(1.16 \pm 0.08) \times 10^3$

Table 6. Comparison of regret on SnAr benchmark (asynchronous) for $T = 100$ and different values of t_{delay} . The best three performances are shown in bold, and the best one in italics. SnAKe consistently achieves regret comparable with BO methods.

delay	0.0-SnAKe	0.1-SnAKe	1.0-SnAKe	ℓ -SnAKe	Random	TS	UCBwLP
5	-4.5 ± 1.3	-5.7 ± 1.4	-4.9 ± 1.2	-4.3 ± 1.1	-2.5 ± 0.7	-5.9 ± 1.2	-6.9 ± 1.4
10	-3.9 ± 0.7	-4.4 ± 0.9	-4.1 ± 0.7	-4.5 ± 1.2	-2.5 ± 0.9	-5.3 ± 1.3	-5.4 ± 1.5
25	-4.0 ± 0.5	-3.7 ± 0.5	-3.7 ± 0.9	-4.0 ± 1.2	-2.3 ± 0.5	-3.7 ± 0.9	-4.1 ± 1.0
50	-2.9 ± 1.2	-3.4 ± 0.6	-3.2 ± 0.8	-3.9 ± 1.2	-2.9 ± 0.8	-3.5 ± 0.9	-4.8 ± 1.3

Table 7. Comparison of cost for SnAr benchmark (synchronous) for different budgets. The best three performances are shown in bold, and the best one in italics. SnAKe consistently achieves lower cost than BO methods, in particular when $\epsilon = 0$.

Budget	0.0-SnAKe	0.1-SnAKe	1.0-SnAKe	ℓ -SnAKe	EI	UCB	PI	Random
10	73 ± 10	85 ± 16	92 ± 12	85 ± 10	104 ± 23	84 ± 12	104 ± 25	83 ± 8
25	$(1.5 \pm 0.4) \times 10^2$	172 ± 26	194 ± 21	188 ± 19	$(2.7 \pm 0.4) \times 10^2$	$(2.2 \pm 0.5) \times 10^2$	275 ± 28	158 ± 8
50	$(2.7 \pm 0.6) \times 10^2$	308 ± 26	$(3.4 \pm 0.5) \times 10^2$	326 ± 26	$(5.7 \pm 0.5) \times 10^2$	$(4.8 \pm 0.5) \times 10^2$	566 ± 34	249 ± 14
100	$(4.1 \pm 0.9) \times 10^2$	$(4.8 \pm 0.6) \times 10^2$	$(4.4 \pm 0.6) \times 10^2$	$(4.7 \pm 0.6) \times 10^2$	$(1.15 \pm 0.06) \times 10^3$	$(9.7 \pm 0.5) \times 10^2$	$(1.11 \pm 0.04) \times 10^3$	349 ± 26

Table 8. Comparison of $\log(\text{regret})$ for SnAr benchmark (synchronous) for different budgets. The best three performances are shown in bold, and the best one in italics. SnAKE achieves the best regret for larger budgets, even if $\epsilon = 0$ (suggesting a lack of local optima).

Budget	0.0-SnAKE	0.1-SnAKE	1.0-SnAKE	ℓ -SnAKE	EI	UCB	PI	Random
10	-1.8 ± 0.4	-2.0 ± 0.4	-1.6 ± 0.8	-2.0 ± 0.5	-1.7 ± 0.6	-2.1 ± 0.8	-1.7 ± 0.7	-1.1 ± 0.6
25	-2.67 ± 0.32	-2.7 ± 0.4	-2.72 ± 0.34	-2.53 ± 0.29	-2.0 ± 0.5	-2.73 ± 0.19	-2.1 ± 0.6	-1.5 ± 0.6
50	-2.99 ± 0.32	-3.0 ± 0.4	-3.0 ± 0.4	-2.91 ± 0.30	-2.49 ± 0.33	-2.95 ± 0.18	-2.3 ± 0.4	-1.8 ± 0.4
100	-3.31 ± 0.04	-3.30 ± 0.05	-3.28 ± 0.11	-3.27 ± 0.09	-2.66 ± 0.35	-3.24 ± 0.05	-2.35 ± 0.35	-1.85 ± 0.21

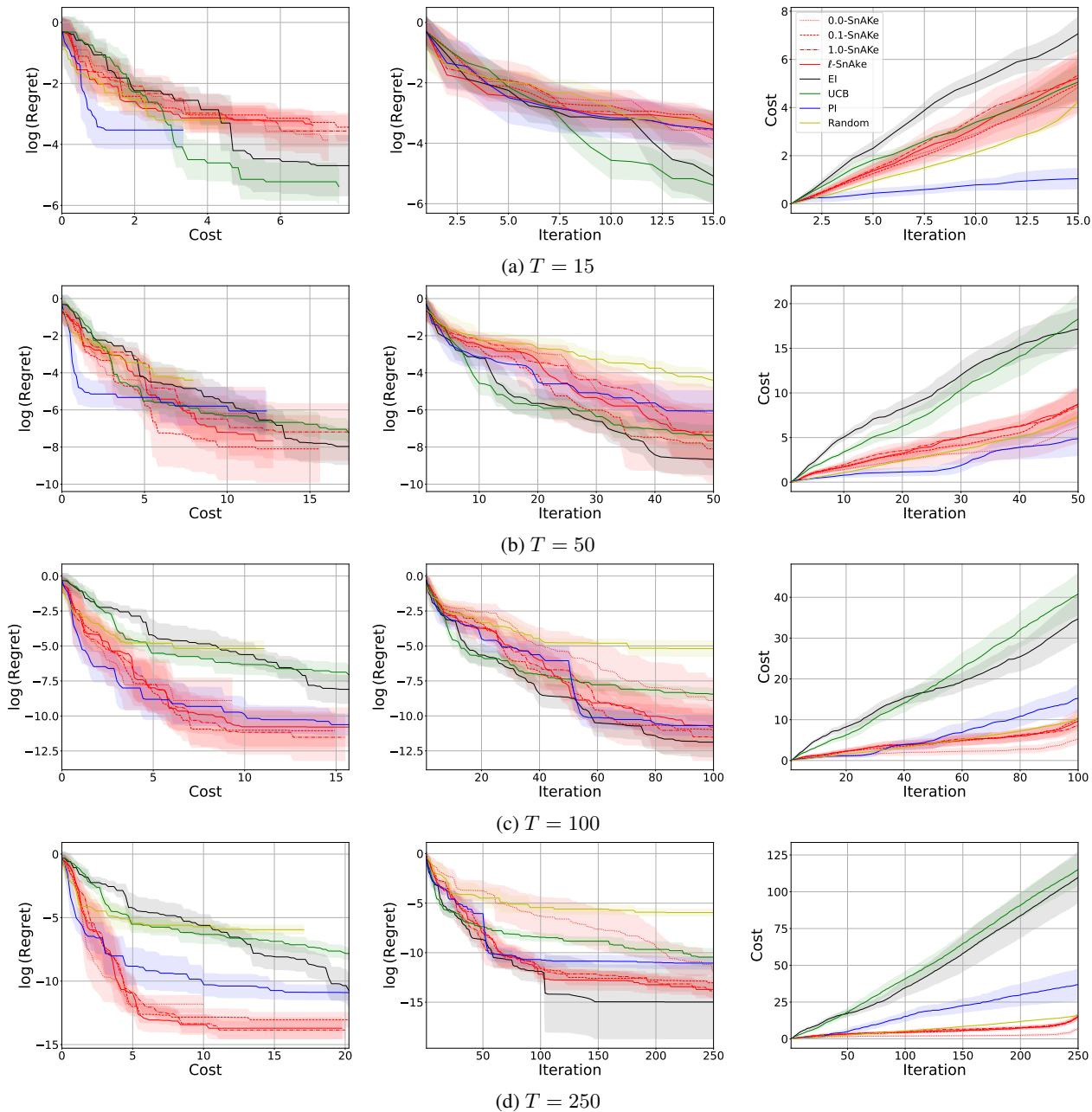


Figure 10. Brainin2D. Each row represents a different budget. The left column shows the evolution of regret against the cost used. The middle column shows the evolution of regret with iterations, and the right columns show the evolution of the 2-norm cost. As we increase the budget, SnAKE outperforms two BO methods in regret, and outperforms all methods in cost. $\epsilon = 0$ gives the smallest cost of all at the expense of some regret.

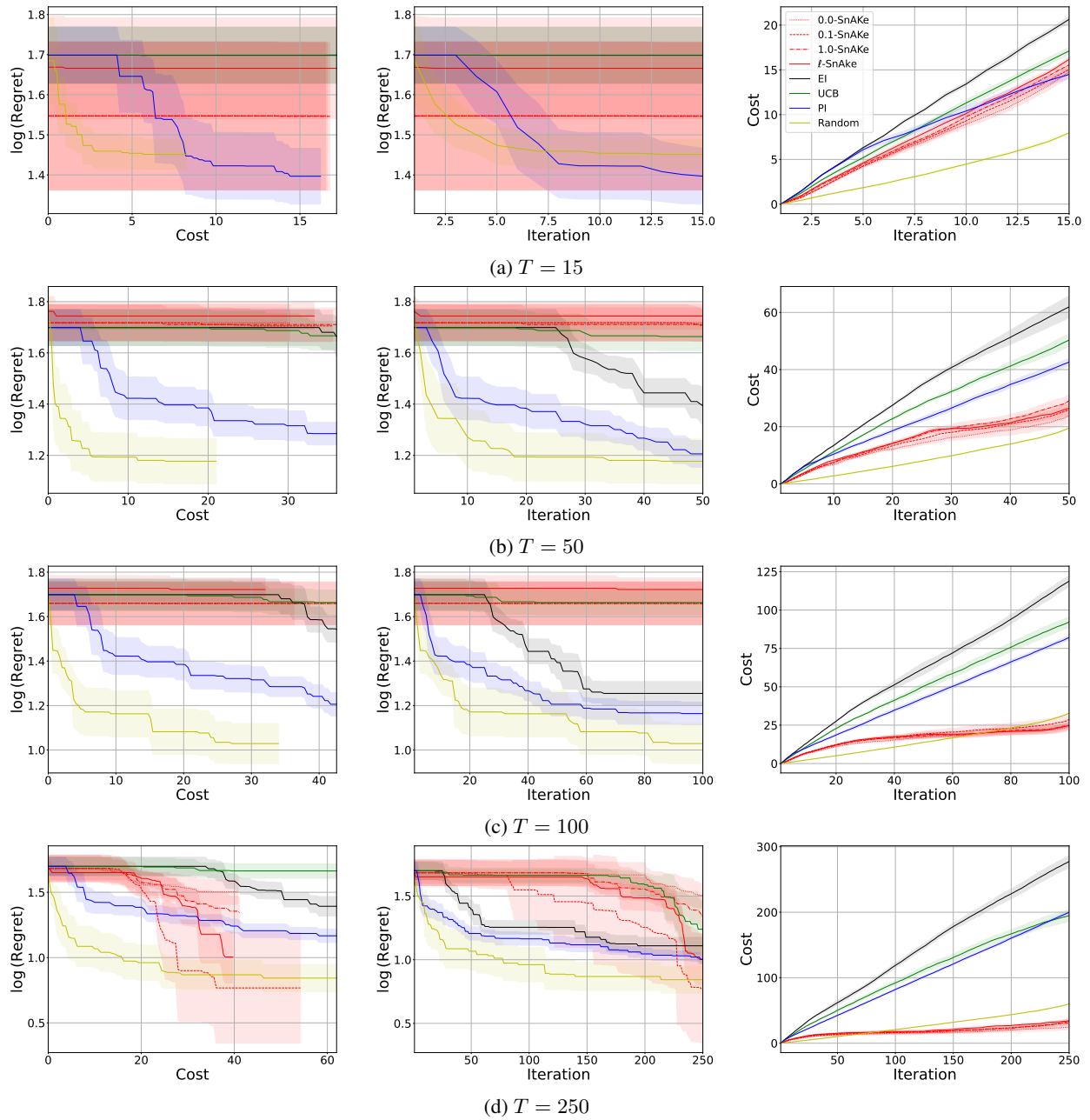


Figure 11. Ackley4D. Each row represents a different budget. The left column shows the evolution of regret against the cost used. The middle column shows the evolution of regret with iterations, and the right columns show the evolution of the 2-norm cost. SnAKE performs badly for smaller budgets, this may be because of the Thompson Sampling (see Figure 19, TS performs very badly in asynchronous Ackley). For the largest budget SnAKE recovers and outperforms all other methods in *both* regret and cost.

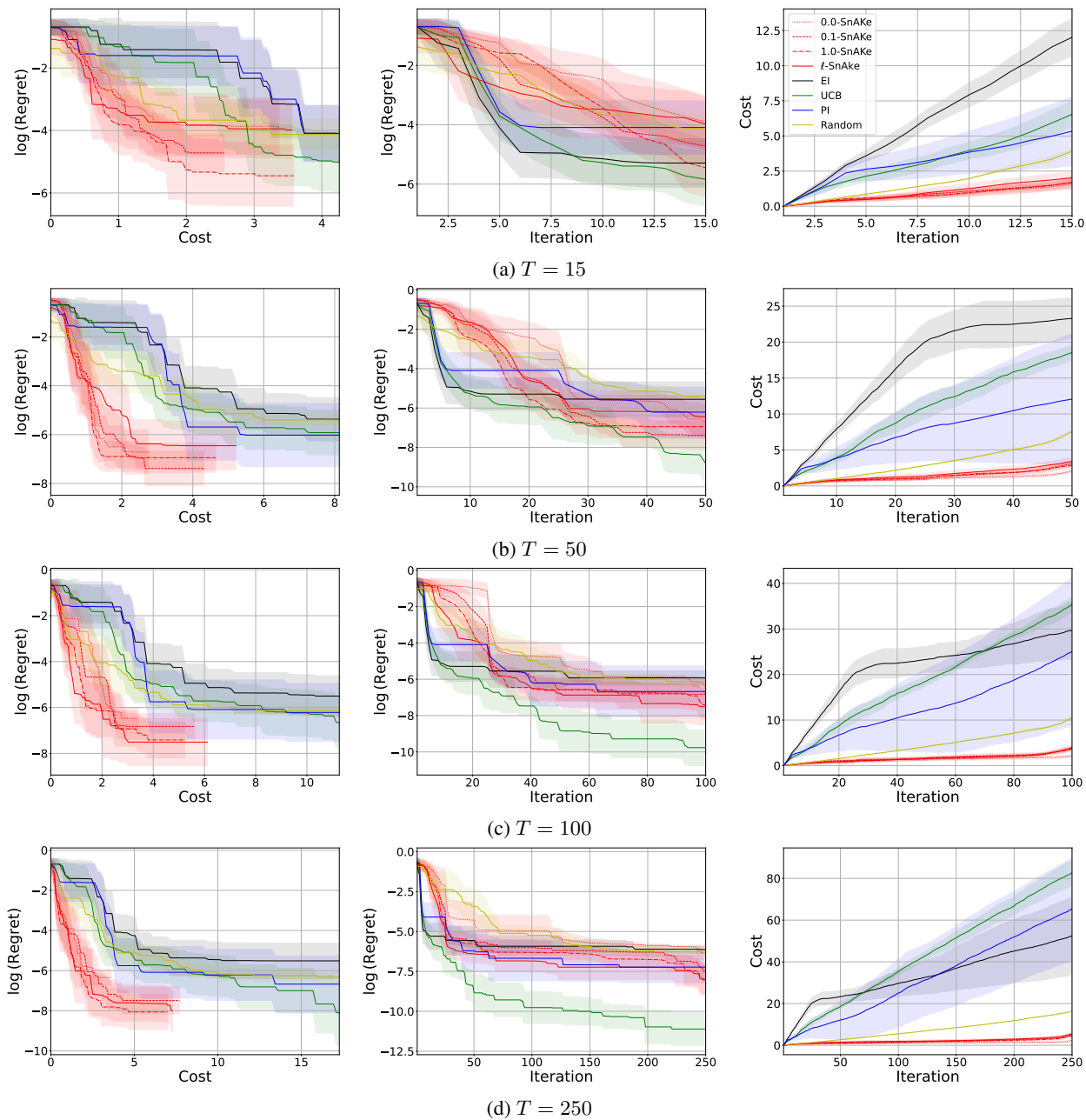


Figure 12. Michaelwicz2D. Each row represents a different budget. The left column shows the evolution of regret against the cost used. The middle column shows the evolution of regret with iterations, and the right columns show the evolution of the 2-norm cost. SnAKE outperforms has regret comparable with other methods for all budgets (UCB outperforms the rest for larger ones). SnAKE achieves significantly less cost at all budgets, this may be due to SnAKE exploring the many local optimums carefully. The first column shows that SnAKE achieves by far the best regret for low cost.

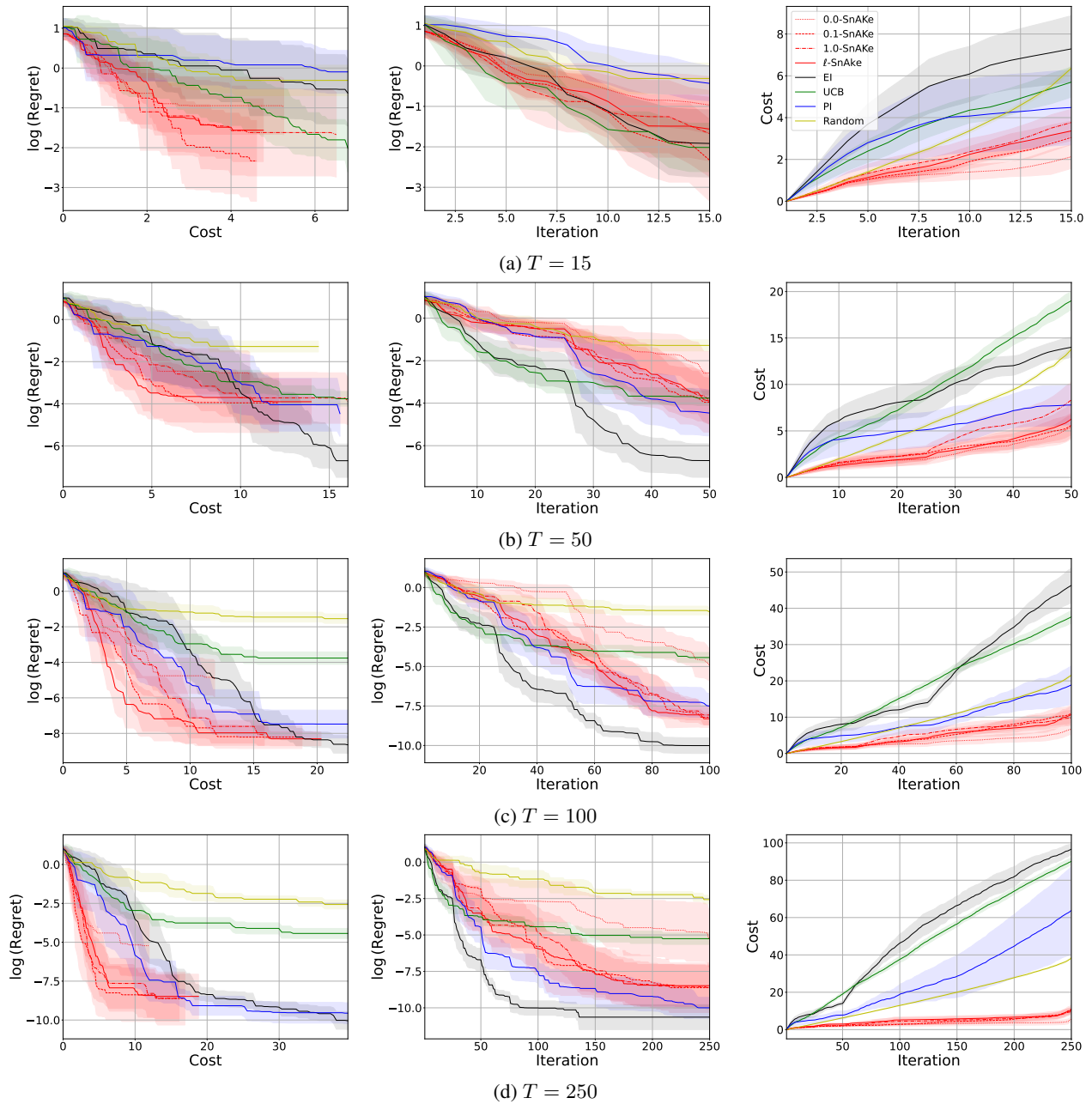


Figure 13. Hartmann3D. Each row represents a different budget. The left column shows the evolution of regret against the cost used. The middle column shows the evolution of regret with iterations, and the right columns show the evolution of the 2-norm cost. Again, SnAKE achieves the best regret at low cost for all budgets. $\epsilon = 0$ struggles in this benchmark, showcasing the impact that Point Deletion can have.

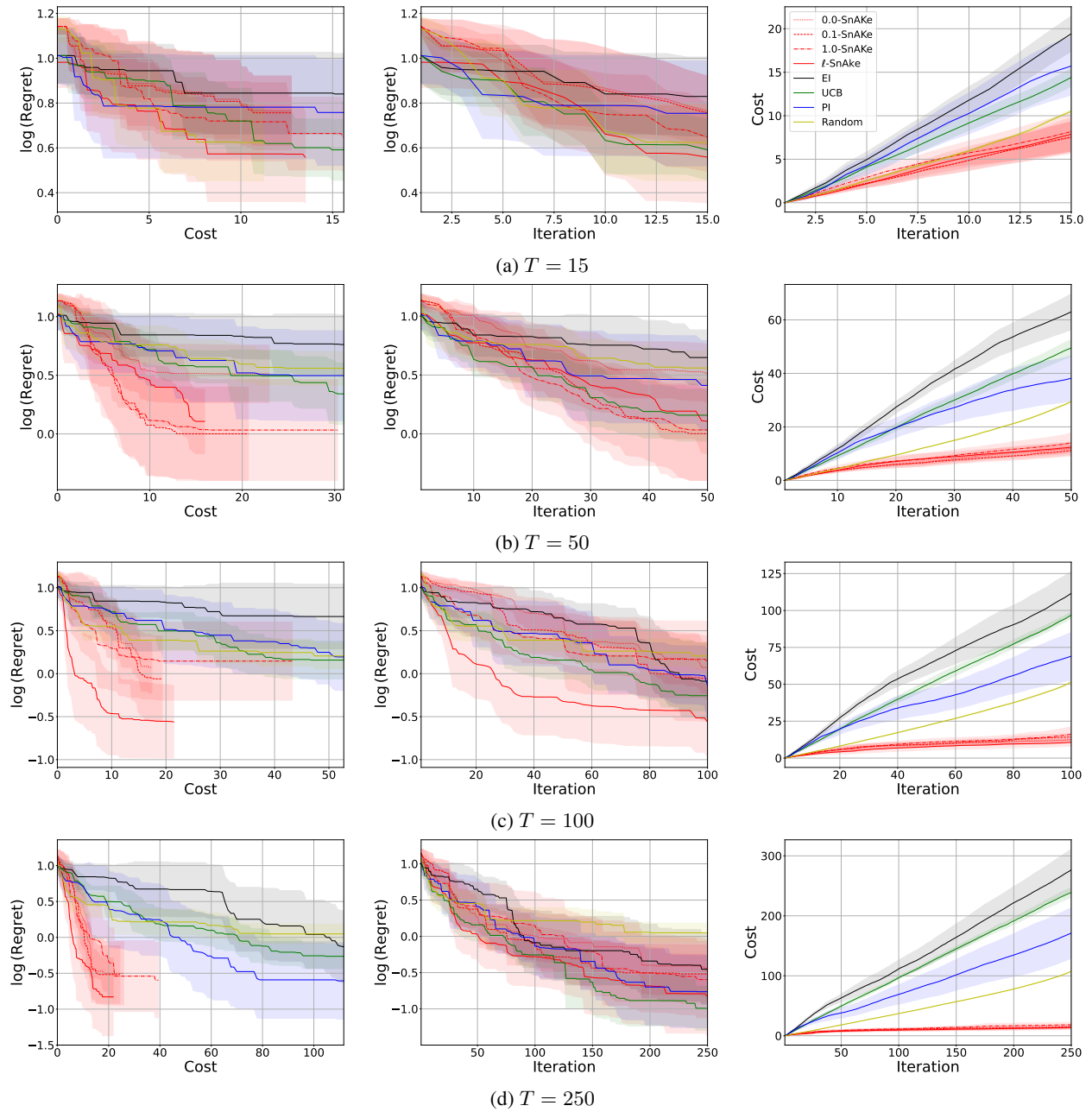


Figure 14. Hartmann6D. Each row represents a different budget. The left column shows the evolution of regret against the cost used. The middle column shows the evolution of regret with iterations, and the right columns show the evolution of the 2-norm cost. A high-dimensional example where SnAKE performs exceedingly well, giving the best regret at low costs for all budgets except $T = 15$. The final cost is considerably lower for SnAKE than any other method.

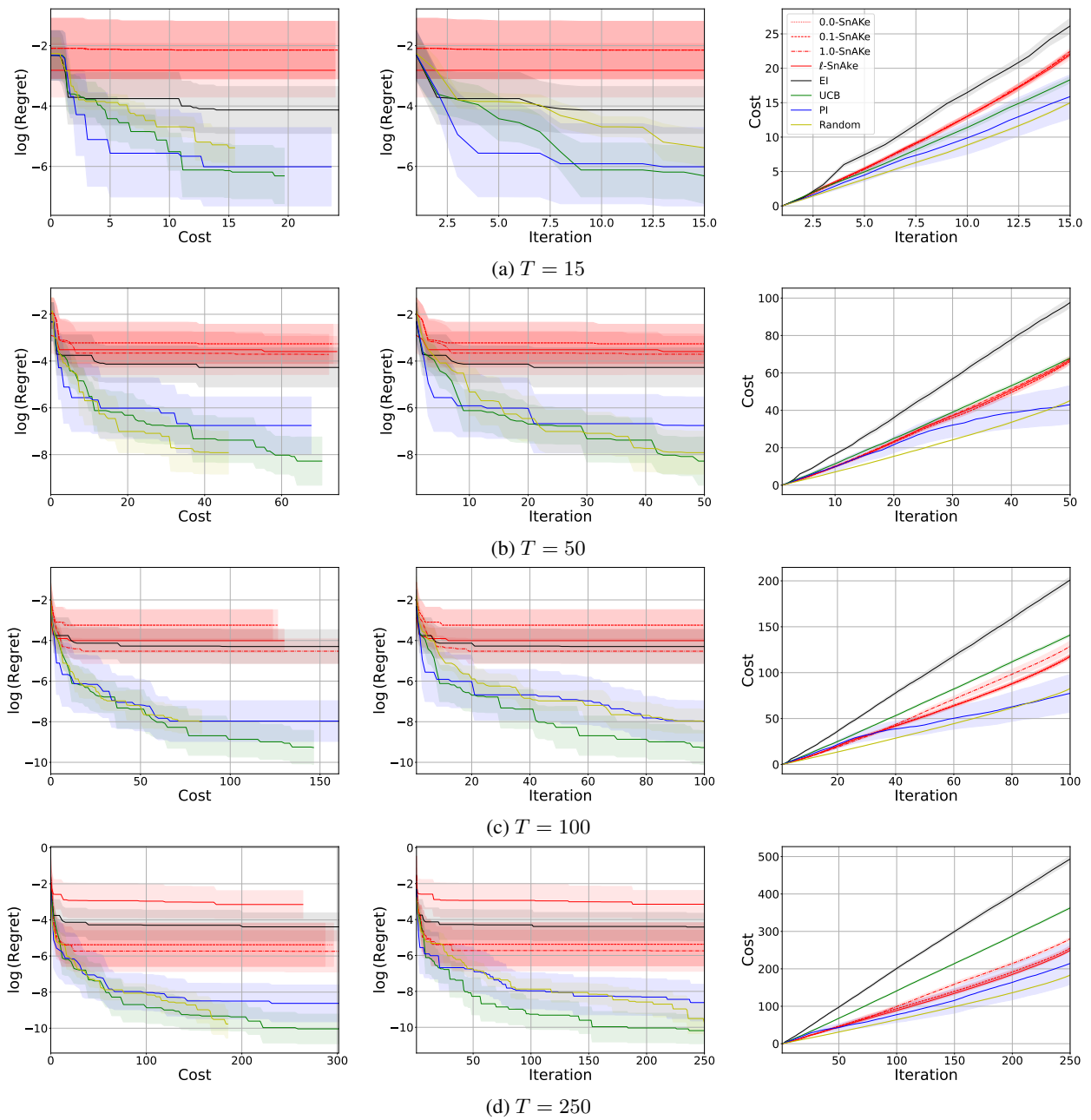


Figure 15. Perm10D. Each row represents a different budget. The left column shows the evolution of regret against the cost used. The middle column shows the evolution of regret with iterations, and the right columns show the evolution of the 2-norm cost. SnAKE struggles in this benchmark, however, EI also struggles. As an interesting observation, if we *did not* update the model, we would achieve a much better performance (as it would be equivalent to Random). We observe this behavior in the asynchronous case, where having a time-delay helps the method perform better (see asynchronous Ackley, Figure 19).

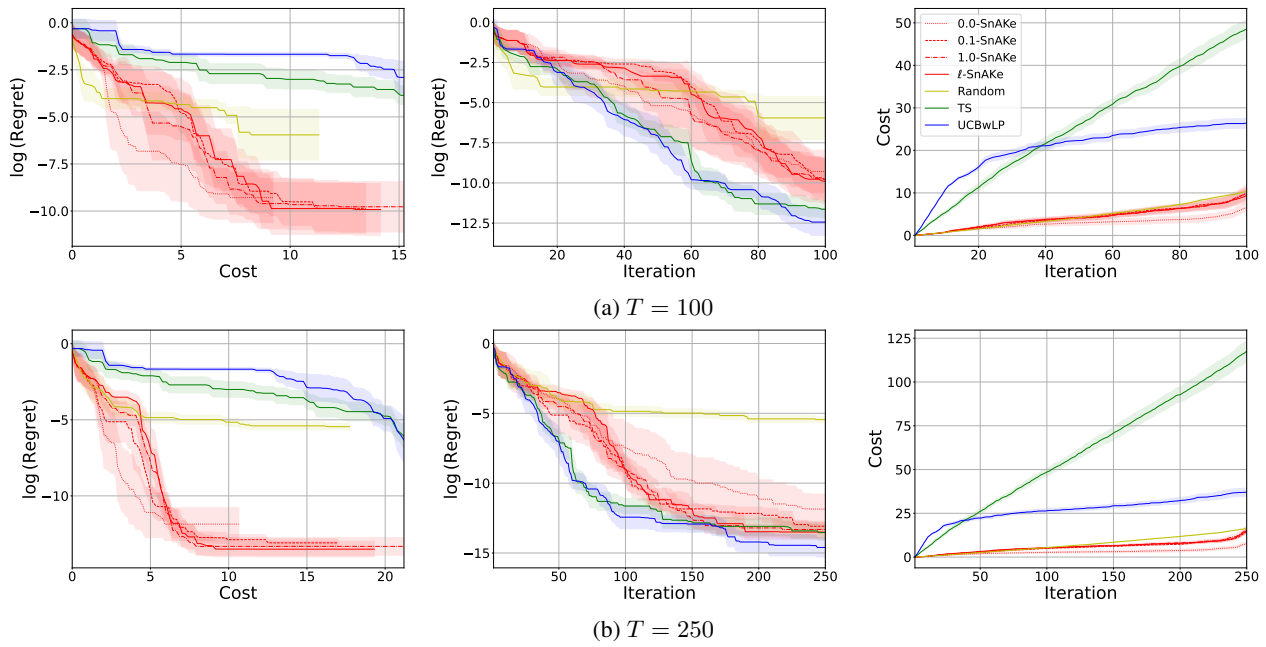


Figure 16. Branin2D (Asynchronous), $t_{delay} = 10$. Each row represents a different budget. The left column shows the evolution of regret against the cost used. The middle column shows the evolution of regret with iterations, and the right columns show the evolution of the 2-norm cost. SnAKE achieves significantly better regret than all other methods at low costs. The final regret of other BO methods is slightly better, but this comes at the expense of much larger cost.

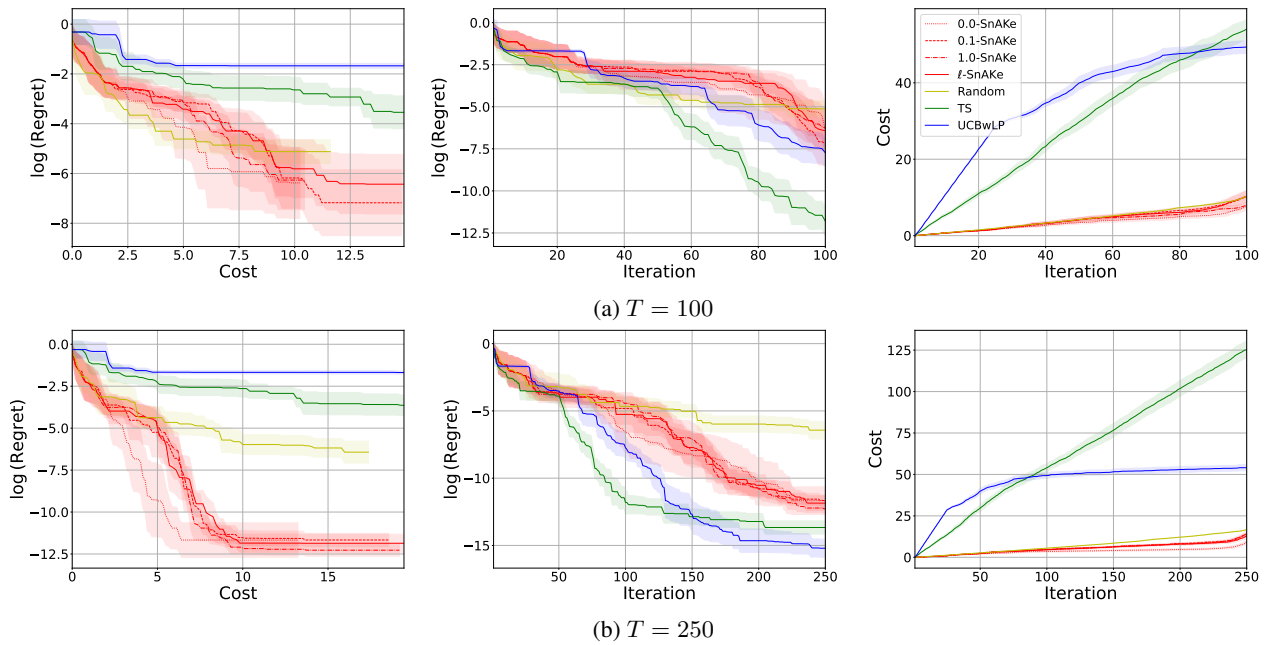


Figure 17. Branin2D (Asynchronous), $t_{delay} = 25$. Each row represents a different budget. The left column shows the evolution of regret against the cost used. The middle column shows the evolution of regret with iterations, and the right columns show the evolution of the 2-norm cost. The results are similar to the shorter delay seen in Figure 16.

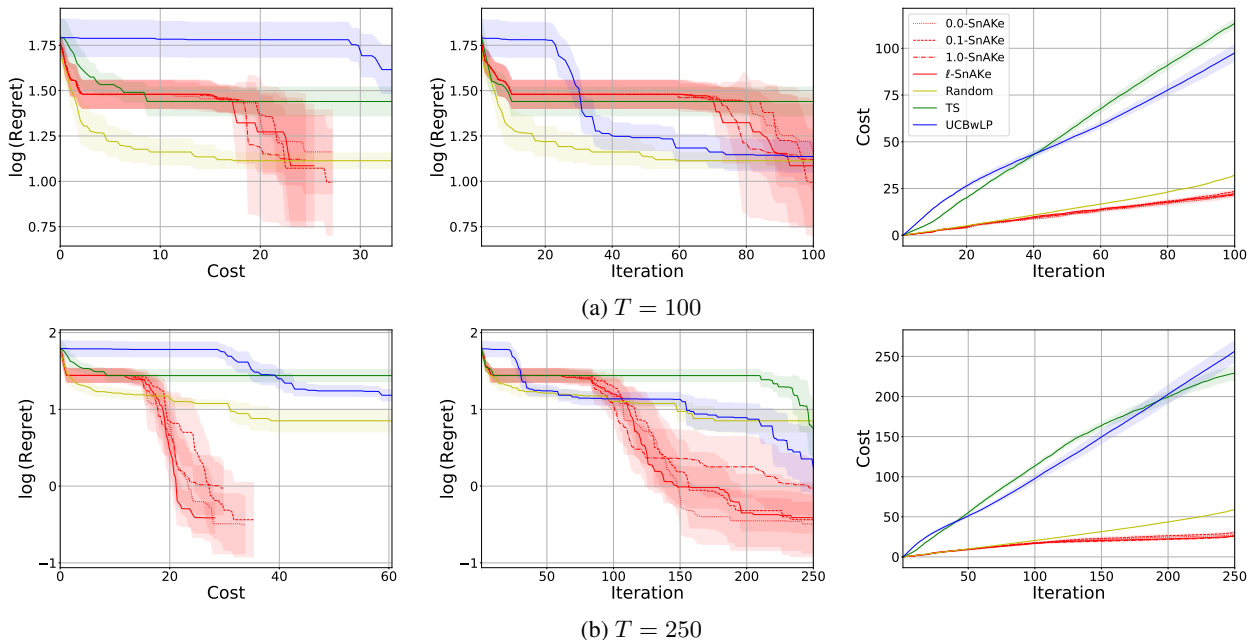


Figure 18. Ackley4D (Asynchronous), $t_{delay} = 10$. Each row represents a different budget. The left column shows the evolution of regret against the cost used. The middle column shows the evolution of regret with iterations, and the right columns show the evolution of the 2-norm cost. For the larger budget, SnAKE outperforms all other methods in both regret and cost. Interestingly, the performance of SnAKE improves when adding delay (see Figure 11 for synchronous results).

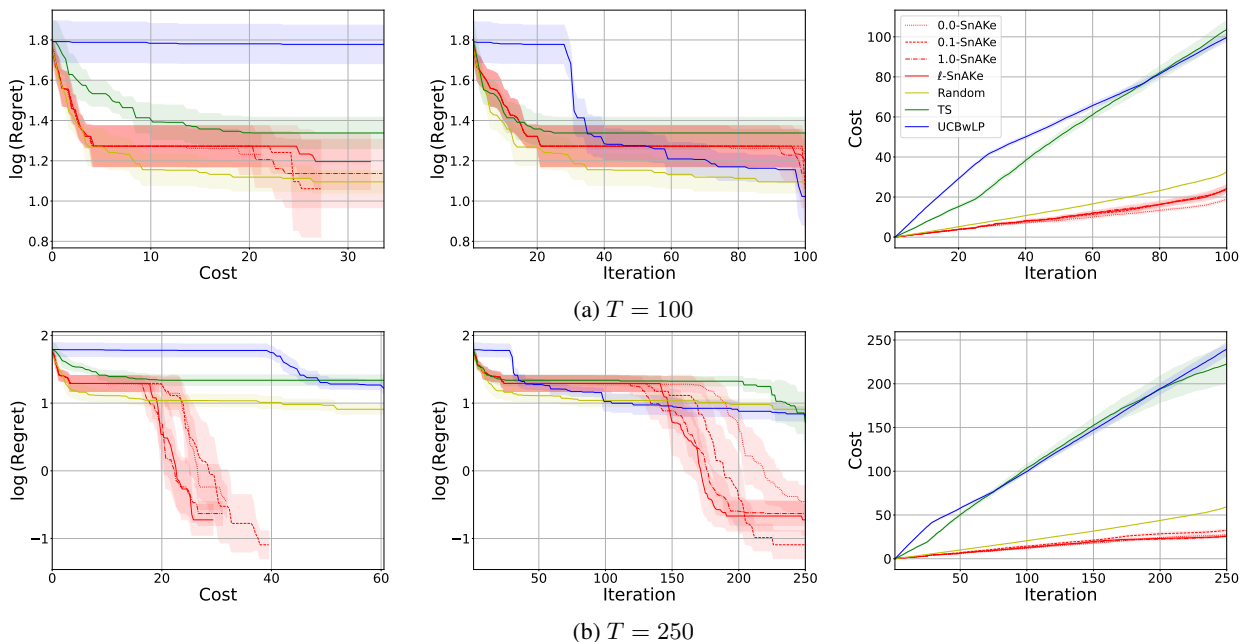


Figure 19. Ackley4D (Asynchronous), $t_{delay} = 25$. Each row represents a different budget. The left column shows the evolution of regret against the cost used. The middle column shows the evolution of regret with iterations, and the right columns show the evolution of the 2-norm cost. Results are similar to the case when $t_{delay} = 10$, see Figure 18.

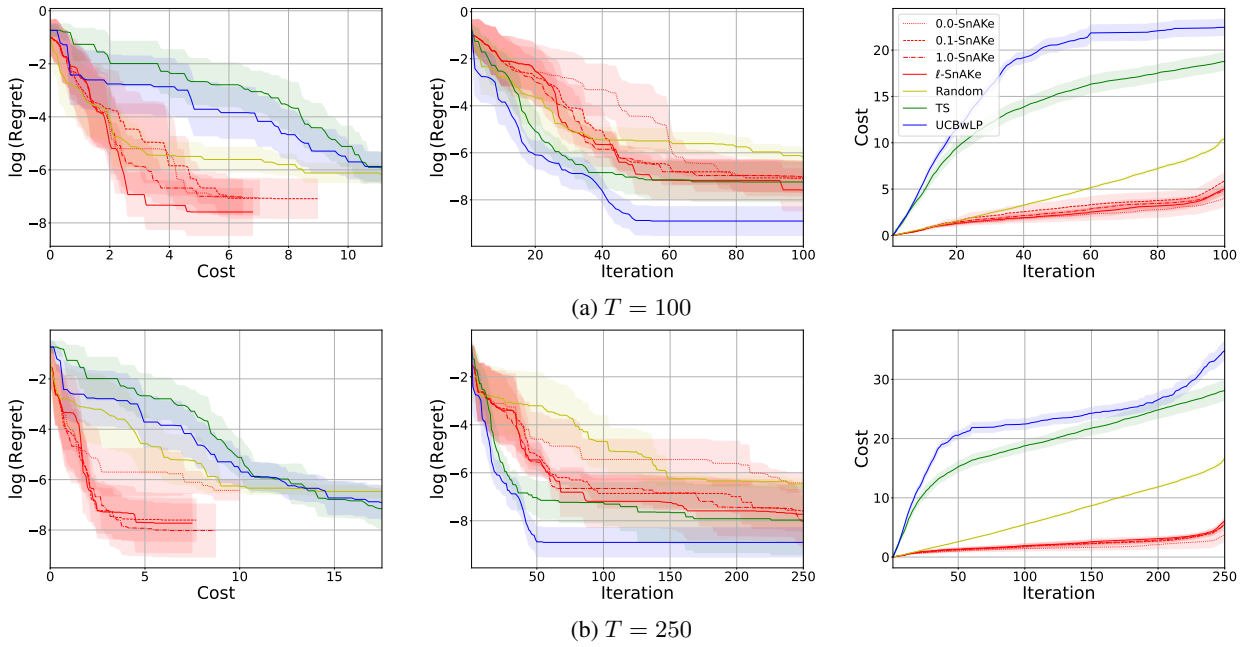


Figure 20. Michaelwicz2D (Asynchronous), $t_{delay} = 10$. Each row represents a different budget. The left column shows the evolution of regret against the cost used. The middle column shows the evolution of regret with iterations, and the right columns show the evolution of the 2-norm cost. For this benchmark, UCBwLP achieves the best regret by far, however, at the cost of significant expense. For low cost, SnAKE achieves much better regret.

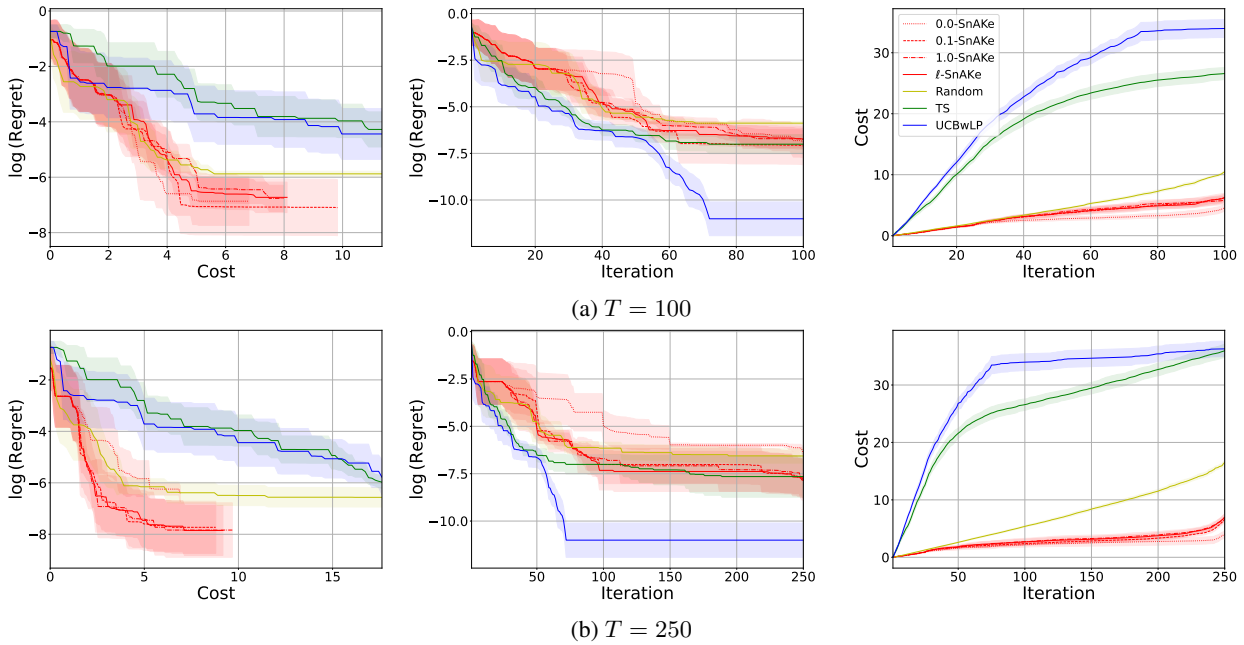


Figure 21. Michaelwicz2D (Asynchronous), $t_{delay} = 25$. Each row represents a different budget. The left column shows the evolution of regret against the cost used. The middle column shows the evolution of regret with iterations, and the right columns show the evolution of the 2-norm cost. Similar results to shorter delay, see Figure 20.

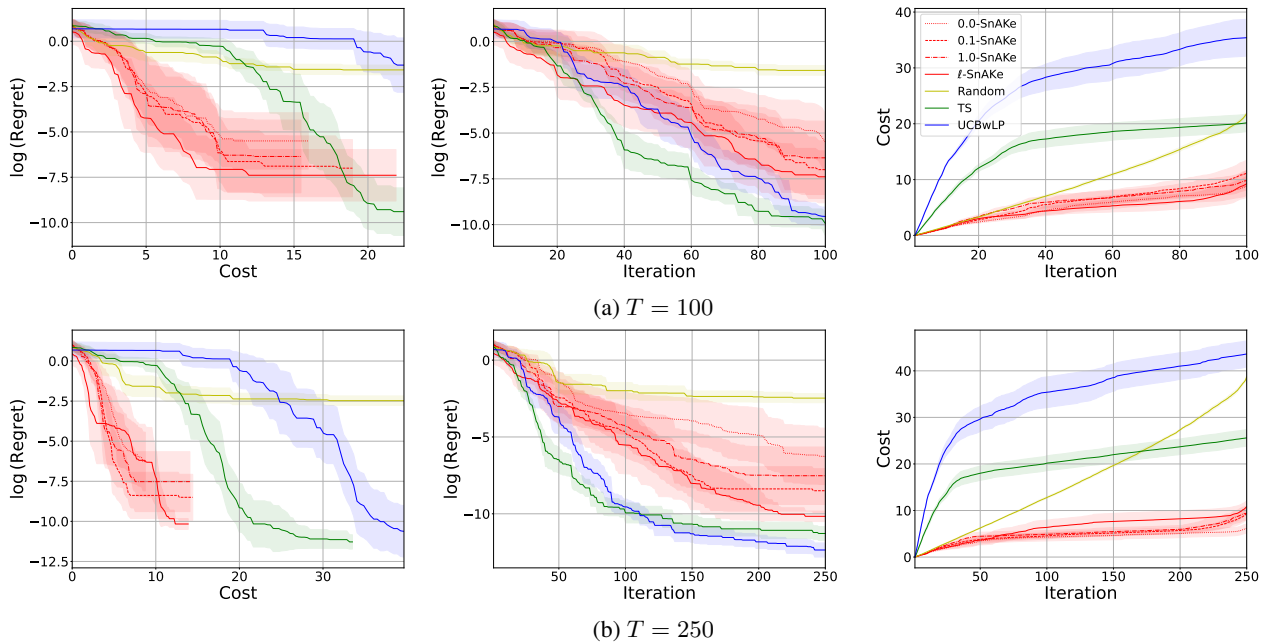


Figure 22. Hartmann3D (Asynchronous), $t_{delay} = 10$. Each row represents a different budget. The left column shows the evolution of regret against the cost used. The middle column shows the evolution of regret with iterations, and the right columns show the evolution of the 2-norm cost. SnAKE achieves the best regret for low cost, with Thompson Sampling also giving a good performance. For the full optimization, UCBwLP achieves the best regret, at the expense of four times the cost of SnAKE.

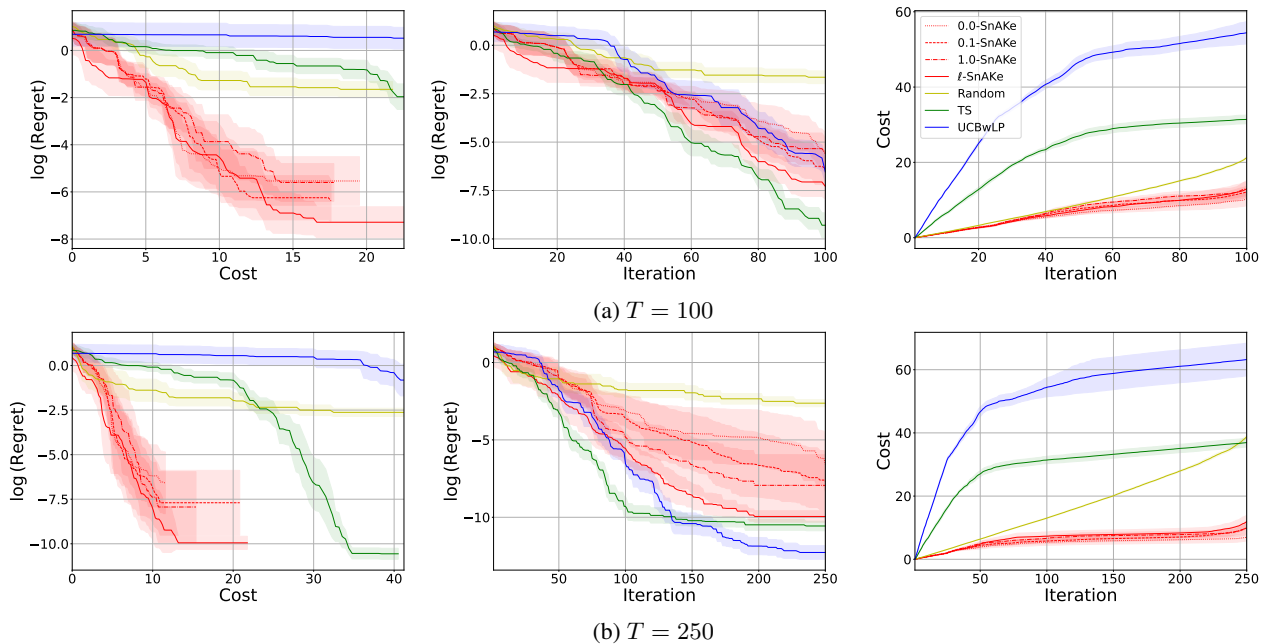


Figure 23. Hartmann3D (Asynchronous), $t_{delay} = 25$. Each row represents a different budget. The left column shows the evolution of regret against the cost used. The middle column shows the evolution of regret with iterations, and the right columns show the evolution of the 2-norm cost. Similar results to the case with smaller delay, see Figure 22.

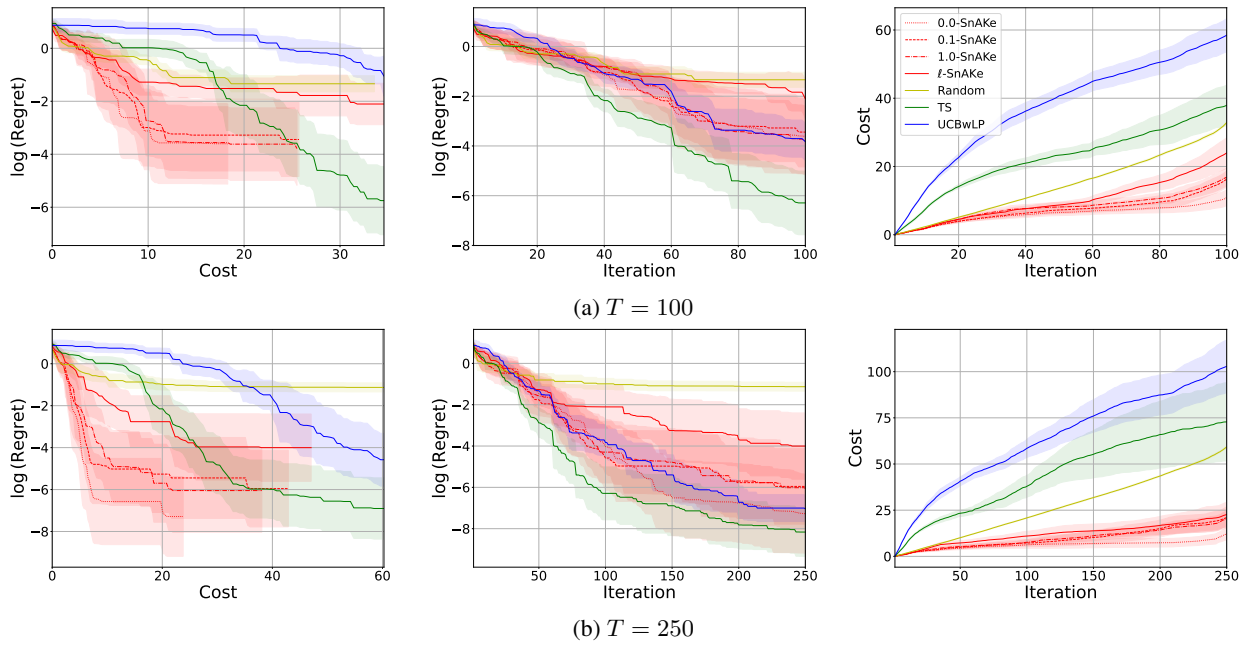


Figure 24. Hartmann4D (Asynchronous), $t_{delay} = 10$. Each row represents a different budget. The left column shows the evolution of regret against the cost used. The middle column shows the evolution of regret with iterations, and the right columns show the evolution of the 2-norm cost. Similar results to other Hartmann benchmarks, see Figure 22.

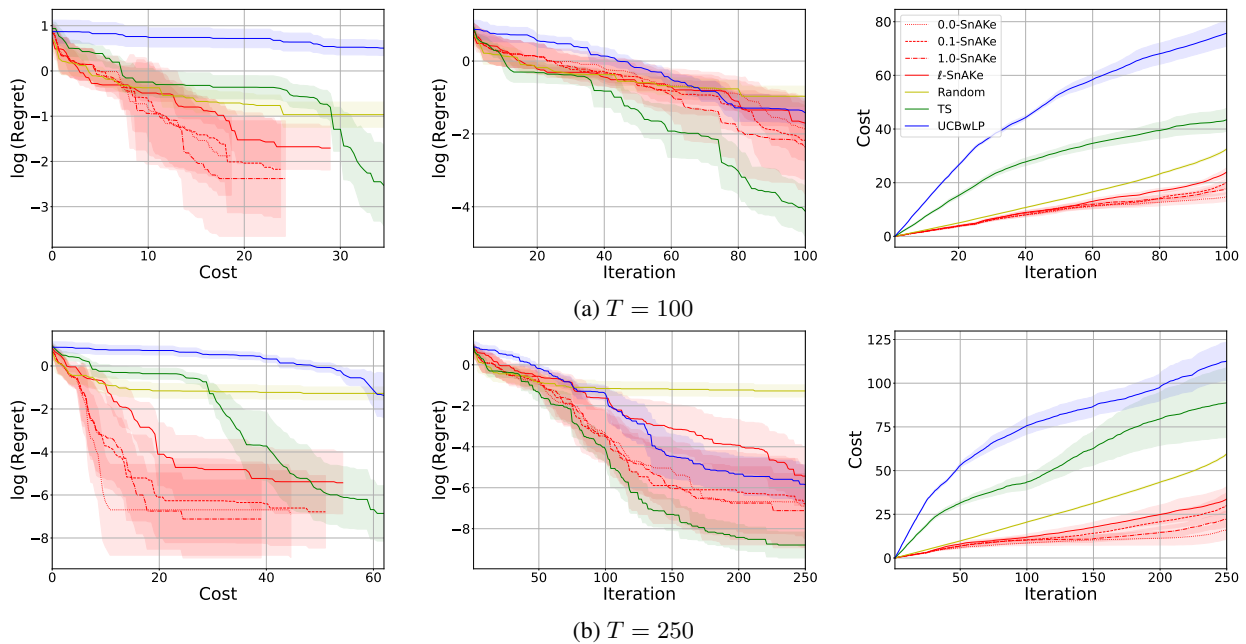


Figure 25. Hartmann4D (Asynchronous), $t_{delay} = 25$. Each row represents a different budget. The left column shows the evolution of regret against the cost used. The middle column shows the evolution of regret with iterations, and the right columns show the evolution of the 2-norm cost. Similar results to other Hartmann benchmarks, see Figure 22.

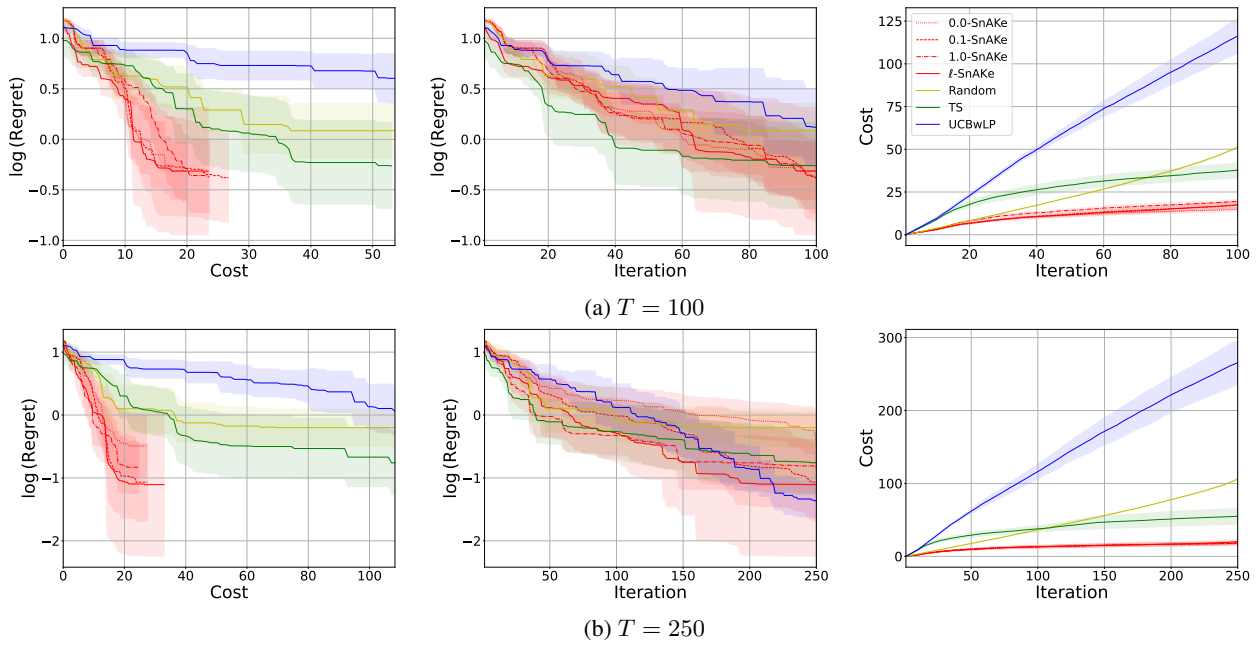


Figure 26. Hartmann6D (Asynchronous), $t_{delay} = 10$. Each row represents a different budget. The left column shows the evolution of regret against the cost used. The middle column shows the evolution of regret with iterations, and the right columns show the evolution of the 2-norm cost. Similar results to other Hartmann benchmarks, see Figure 22.

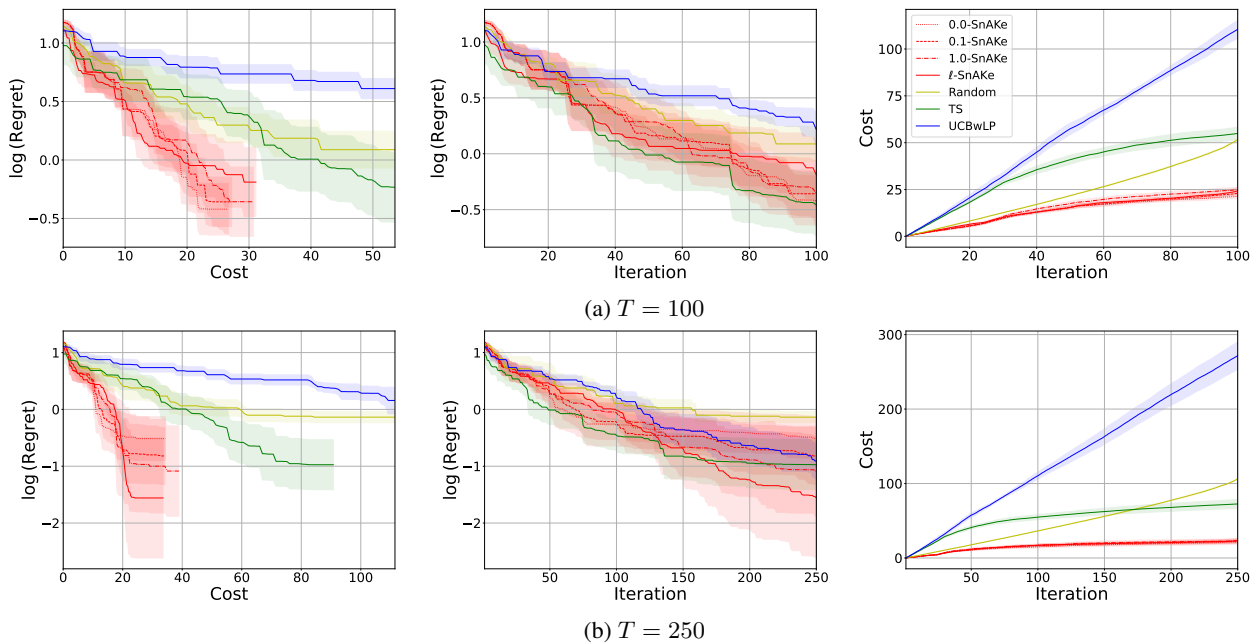


Figure 27. Hartmann6D (Asynchronous), $t_{delay} = 25$. Each row represents a different budget. The left column shows the evolution of regret against the cost used. The middle column shows the evolution of regret with iterations, and the right columns show the evolution of the 2-norm cost. Similar results to other Hartmann benchmarks, see Figure 22.

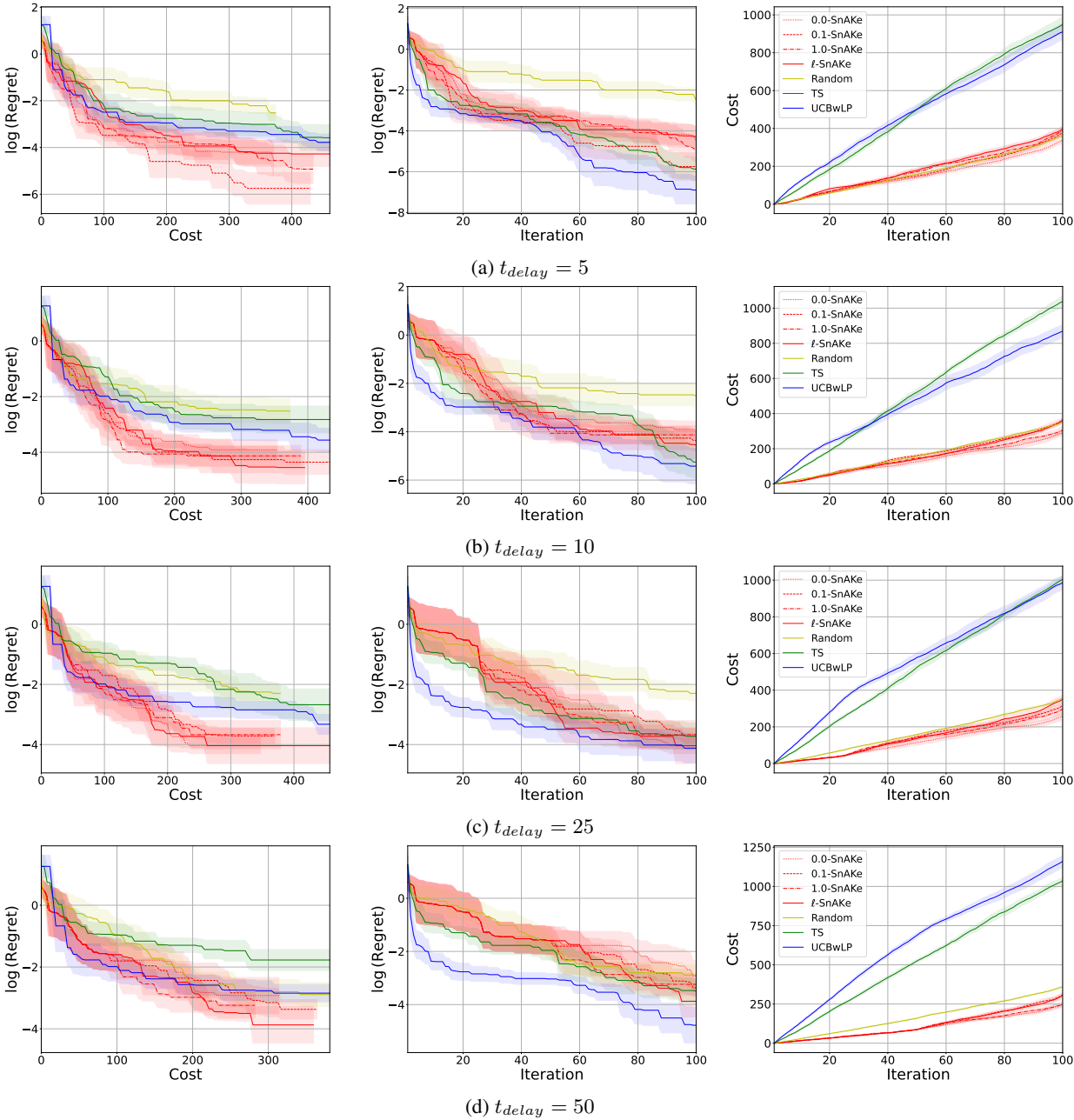


Figure 28. SnAr benchmark (Asynchronous) with $T = 100$. Each row represents a different t_{delay} . The left column shows the evolution of regret against the cost used. The middle column shows the evolution of regret with iterations, and the right columns show the evolution of the cost as defined in Section 4.2. SnAKE achieves the best regret at low cost for all budgets. For the full optimization, UCBwLP is best in regret, but SnAKE has much lower input costs.

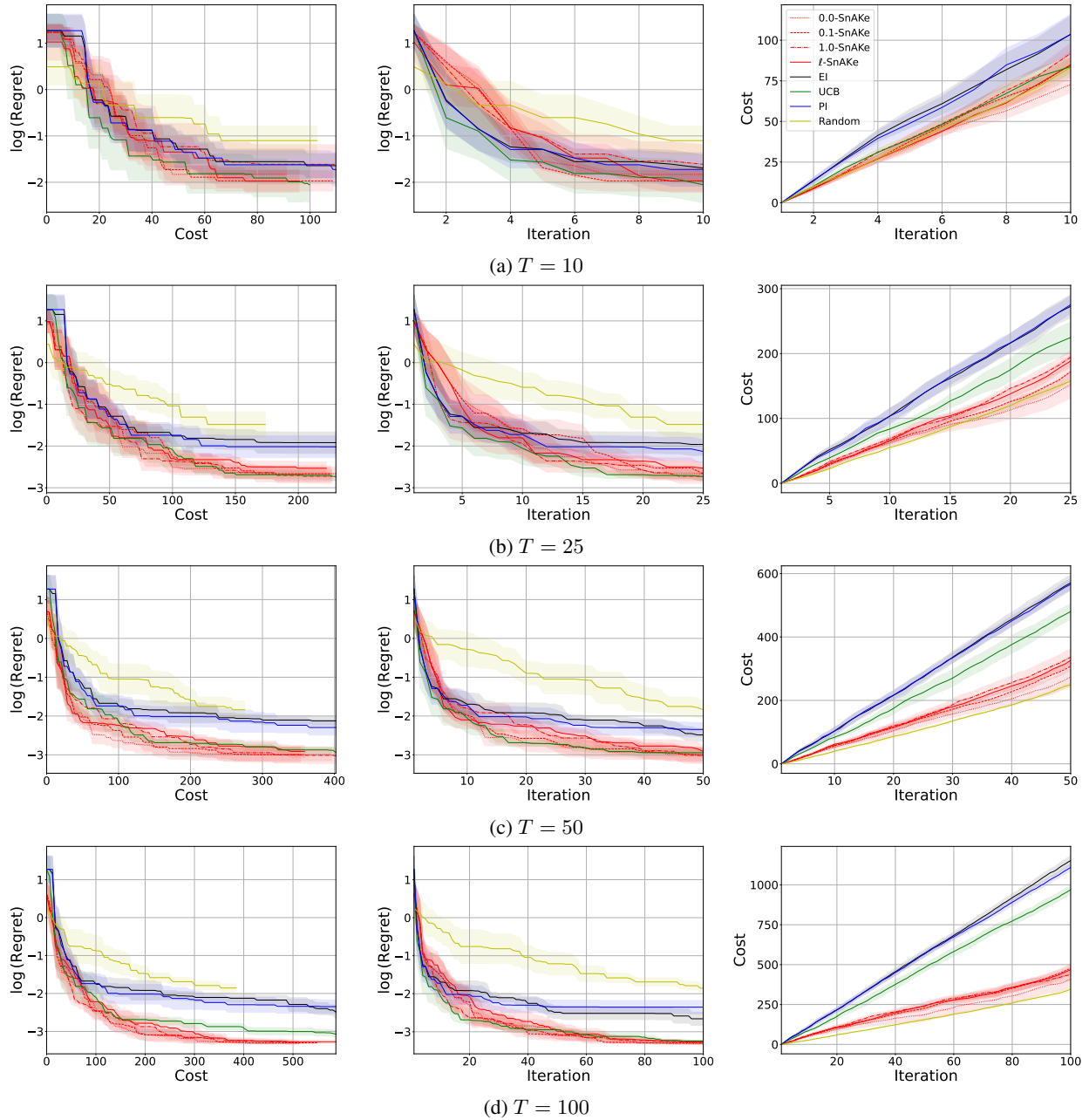


Figure 29. SnAr benchmark (synchronous, $t_{delay} = 1$). Each row shows a different budget. The left column shows the evolution of regret against the cost used. The middle column shows the evolution of regret with iterations, and the right columns show the evolution of the cost as defined in Section 4.2. SnAKE is the only method achieving low regret and low cost especially for larger budgets.